Dynamic hidden-variable network models

Harrison Hartle[1], Fragkiskos Papadopoulos[2], and Dmitri Krioukov[1,3]

[1]*Network Science Institute, Northeastern University, Boston, 02115 Massachusetts, USA*
[2]*Department of Electrical Engineering, Computer Engineering and Informatics, Cyprus University of Technology, 3036 Limassol, Cyprus*
[3]*Northeastern University, Departments of Physics, Mathematics, and Electrical & Computer Engineering, Boston, 02115 Massachusetts, USA*

Models of complex networks often incorporate node-intrinsic properties abstracted as hidden variables. The probability of connections in the network is then a function of these variables. Real-world networks evolve over time and many exhibit dynamics of node characteristics as well as of linking structure. Here we introduce and study natural temporal extensions of static hidden-variable network models with stochastic dynamics of hidden variables and links. The dynamics is controlled by two parameters: one that tunes the rate of change of hidden variables and another that tunes the rate at which node pairs reevaluate their connections given the current values of hidden variables. Snapshots of networks in the dynamic models are equivalent to networks generated by the static models only if the link reevaluation rate is sufficiently larger than the rate of hidden-variable dynamics or if an additional mechanism is added whereby links actively respond to changes in hidden variables. Otherwise, links are out of equilibrium with respect to hidden variables and network snapshots exhibit structural deviations from the static models. We examine the level of structural persistence in the considered models and quantify deviations from staticlike behavior. We explore temporal versions of popular static models with community structure, latent geometry, and degree heterogeneity. While we do not attempt to directly model real networks, we comment on interesting qualitative resemblances to real systems. In particular, we speculate that links in some real networks are out of equilibrium with respect to hidden variables, partially explaining the presence of long-ranged links in geometrically embedded systems and intergroup connectivity in modular systems. We also discuss possible extensions, generalizations, and applications of the introduced class of dynamic network models.

I. INTRODUCTION

Networks are ubiquitous in nature [1–9], and their study relies heavily on the mathematical and computational analysis of simple models [10,11], typically in the form of random networks built according to some stochastic rules. In many models, nodes are assigned characteristics (such as fitnesses [12,13] or spatial coordinates in a physical [14] or latent space [15–17]), which in turn affect the network's structural formation. Such models fall under the umbrella of *hidden-variable* (HV) models [18] because they depend on internal node characteristics that are only implicitly expressed by the network structure through effects on link formation. Usually, HVs are not externally specified as parameters; rather, their probability distribution is specified [12,19] and they are sampled during the network's formation. Two sources of randomness underly such networks: the random HVs of nodes and the random formation of edges given those HVs. In general, HV models are defined by the following procedure:

(1) A random HV configuration H is drawn with probability density $\rho(H)$ from a set of possible HV configurations $\mathcal{H}$.

(2) Graph G is then drawn with conditional probability $\mathbb{P}(G|H)$ from a set of possible graphs $\mathcal{G}$.

As a result, the overall probability of sampling any particular graph $G \in \mathcal{G}$ is equal to

$$\mathbb{P}(G) = \int_{\mathcal{H}} \mathbb{P}(G|H)\rho(H)dH. \qquad (1)$$

HV models, due to their capacity to encode nodewise heterogeneity, are in many cases capable of exhibiting more structural realism than models without HVs. For example, HVs underly network models incorporating realistic features such as community structure (stochastic block models (SBMs) [20]), latent geometry (random geometric graphs (RGGs) [21]), and degree heterogeneity (soft configuration models (SCMs) [22]).

However, such models do not capture the *dynamics* of node characteristics nor the impact thereof on network structure. The influence of dynamic node states on evolving link structures has been investigated in the context of *adaptive networks* [23–28], but in that case node states arise due to a highly complex feedback, interacting with one another through co-evolving links. Such models are more realistic and have interesting features but they do not directly explore the impact of dynamic node properties on dynamic network structure.

There is a wide abundance of real-world examples of dynamic node properties influencing the dynamics of network structure, such as:

(a) changing habits, interests, jobs, and other attributes of people in social networks [29],

(b) changing geospatial coordinates of organisms during formation of social ties, group-memberships, and pathogenic contact networks [30–34],

(c) changing phenotypic traits of species as they biologically evolve in ecological networks [35,36],

(d) changing marketing and administrative strategies of entities in economic networks [37,38],

(e) changing demographic and infrastructural characteristics of cities in evolving highway and airport networks [39–41],

(f) changing gene-expression levels of neurons in developing connectomes [42,43],

(g) changing consumption-levels of residential nodes in evolving power grids [44,45], and

(h) changing displayed content of websites on the evolving world-wide web [46,47].

These examples motivate the development of a simple modeling framework describing the impact of dynamic node characteristics on dynamic link structures. Such a framework would provide a temporal analog of how node properties influence network structure in HV models. In fact, it is standard practice to derive temporal versions of static-network concepts [48–66], as has been done for several models of static networks with hidden variables such as SBMs [67–73].

Motivated by these considerations, here we study temporal extensions of general static hidden-variables models (SHVMs) obtained by introducing dynamics of hidden variables and of links. In these models, each node has an evolving HV and each node pair has a pairwise *affinity* (equal to the connection probability in the SHVM), which is a function of the HVs of both nodes. Pairwise affinities evolve over time due to their dependence on a pair of evolving HVs. The network itself evolves via node pairs being selected to reevaluate their connections, resampling them with connection probability equal to the pair's affinity at the moment of reevaluation. These systems are governed by just two parameters beyond those of any static model: a rate of HV dynamics σ and a rate of link resampling ω.

We find that these models have snapshots that are statistically equivalent to networks generated from the static model if:

(a) the link-resampling rate is sufficiently larger than the rate of HV dynamics, or

(b) if we add an additional dynamic mechanism whereby links actively respond to changes in HVs.

We also identify the conditions under which model networks evolve *gradually*, i.e., exhibit link persistence, and evaluate qualitative resemblances of snapshots to some real networks which arise as *deviations* from static-model behavior. We obtain analytical and numerical results for effective connection probabilities (the probability of a node pair being connected given their *current* HV values), directly quantifying deviations from static-model behavior in each case.

The family of models we introduce is demonstrated to have wide generality, as exemplified by temporal extensions of four different static models with HVs: SBMs [20], RGGs [21], SCMs [22], and hyperbolic graphs [15]. These examples relate to, and partially encompass, several models of

networks with dynamic node properties that have been previously studied—for instance, dynamic latent space models [74–77], dynamic RGGs [78,79], and dynamic SBMs [72,73]. The framework we study is also widely generalizable to other contexts.

Our study takes a step toward realistic modeling of dynamic networks with dynamic node properties. It introduces a family of temporal network models that extends SHVMs to the temporal setting, providing theoretical insight into the kinds of structure that can emerge as a consequence of the influence of HV dynamics on network-structure dynamics. The framework can be used for studying real-world temporal networks under the null hypothesis that physical or latent *dynamic* hidden variables drive the dynamics of network structure. Additionally, motivated by the phenomenology emerging in these models, we speculate that links in some real systems are *out of equilibrium* with respect to HVs, partially explaining the presence of long-ranged links in geometrically embedded systems and intergroup connectivity in modular systems.

In Sec. II, we describe the properties that we use to characterize the models we introduce. We then introduce the static and temporal hidden-variables model (THVM) families in Sec. III, followed by various limiting regimes in Sec. IV. Section V provides several examples illustrating temporal HV models. We then consider a variant of the family of models in Sec. VI, incorporating an additional dynamic mechanism that enforces static-model connection probabilities. The final sections are dedicated to descriptions of related work (Sec. VII) and a discussion of our results and the implications thereof (Sec. VIII). Appendices provide the details of several calculations and procedures left out of the main text.

II. DESIRED PROPERTIES OF DYNAMIC HIDDEN-VARIABLE MODELS

This section outlines the properties that we use to characterize the family of dynamic HV models that we introduce. Our goal is to construct natural temporal versions of static networks with HVs and to understand the consequences of having introduced such dynamics. Our approach is via a Markov chain on graphs and HV configurations, with sources of randomness in the original static model being replaced by random *processes* in the temporal model.

Specifically, given an SHVM, i.e., a probability density on HV configurations $H \in \mathcal{H}$ and a conditional probability distribution on graphs $G \in \mathcal{G}$ given H, the temporal extension yields a probability distribution/density on *temporal sequences* of graphs and HV configurations, denoted $\mathbf{G} = \{G^{(t)}\}_{t=1}^{T} \in \mathcal{G}^T$ and $\mathbf{H} = \{H^{(t)}\}_{t=1}^{T} \in \mathcal{H}^T$, respectively. We will evaluate the conditions under which models within our framework satisfy the following properties:

(a) *Equilibrium property.* The marginal probability of a graph at any timestep is identical to its probability in the static model; likewise for HVs.

(b) *Persistence property.* The level of structural persistence over time—quantified by, e.g., any graph similarity measure between graphs at adjacent time steps—is high relative to the null expectation (of two independent and identically distributed (i.i.d.) static-model samples).

(c) *Qualitative realism.* The graph-structure, HV geometry (e.g., link lengths), and/or dynamic behaviors resemble observed characteristics of some real-world systems at a qualitative level.

If the equilibrium property is satisfied, the temporal network in question is a strict extension of the static model—individual snapshots are then indistinguishable from static-model realizations. If the equilibrium property is *not* satisfied, snapshots *deviate* from the static model, the resulting phenomenology of which we seek to understand. The persistence property holding implies a *gradually* evolving network, without sudden structural transitions between networks at adjacent time steps. The persistence property can be quantified by application of graph similarity measures [80] to graphs at neighboring time steps. In most cases, the level of structural persistence is tunable, making the level of satisfaction of the persistence property fall along a continuum. The highest accessible persistence values arise when the graph is completely unchanging over time, whereas the lowest accessible persistence values correspond to graphs that are completely resampled each time step. To have qualitative realism simply means that the system exhibits some characteristics and behaviors that are analogous to real-world systems—regardless of whether the detailed mechanisms are realistic or quantitatively accurate. In particular, we are interested in qualitative features relating to the dynamics of node characteristics and the effects of such dynamics on a network's structural evolution.

III. MODELING FRAMEWORK

This section provides an overview of our modeling approach and then defines static and TVHMs. We first describe our approach to constructing temporal extensions of static models, which produce length-T sequences of graphs $\mathbf{G}$ with a probability conditioned on a length-T sequence of HV configurations $\mathbf{H}$. The latter arises from Markovian dynamics [81,82] governed by conditional probability density $\mathcal{P}_H(H^{(t+1)}|H^{(t)})$. The initial configuration $H^{(1)}$ is sampled from the static-model HV density $\rho(H^{(1)})$. Markovian dynamics yields a temporally joint probability density $p(\mathbf{H})$ as a product:

$$p(\mathbf{H}) = \rho(H^{(1)}) \prod_{t=1}^{T-1} \mathcal{P}_H(H^{(t+1)}|H^{(t)}). \quad (2)$$

Given $\mathbf{H}$, the graph sequence $\mathbf{G}$ is produced via a Markov chain with transition probability having auxiliary $\mathbf{H}$ dependence, $\mathcal{P}_G(G^{(t+1)}|G^{(t)}, \mathbf{H})$. Herein, we primarily consider graph dynamics with $\mathbf{H}$ dependence of the form $\mathcal{P}_G(G^{(t+1)}|G^{(t)}, H^{(t+1)})$ but also consider dynamics of the form $\mathcal{P}_G(G^{(t+1)}|G^{(t)}, H^{(t+1)}, H^{(t)})$ in Sec. VI. In general, we could consider any choice of $\mathbf{H}$ dependence—as long as $G^{(t)}$ is not influenced by $H^{(t')}$ for any $t' > t$, since that would entail graph structure at time t being dependent on HVs at future times $t' > t$. The initial graph $G^{(1)}$ is sampled from the static-model conditional probability $\mathbb{P}(G^{(1)}|H^{(1)})$. The $\mathbf{H}$-conditioned temporally joint graph probability distribution

$P(\mathbf{G}|\mathbf{H})$ is then given by

$$P(\mathbf{G}|\mathbf{H}) = \mathbb{P}(G^{(1)}|H^{(1)}) \prod_{t=1}^{T-1} \mathcal{P}_G(G^{(t+1)}|G^{(t)}, \mathbf{H}). \quad (3)$$

Altogether, the temporally joint graph probability distribution is given by

$$P(\mathbf{G}) = \int_{\mathcal{H}^T} P(\mathbf{G}|\mathbf{H}) p(\mathbf{H}) d\mathbf{H}, \quad (4)$$

which is the temporal extension of Eq. (1).

It is this strategy that underlies all temporal extensions of static models that we consider. Static graphs without hyperparameters may also be included by disregarding $\mathbf{H}$ above, leaving only Eq. (3), which becomes a general Markov chain on graphs governed by $\mathcal{P}_G(G^{(t+1)}|G^{(t)})$. Note that $\mathbf{G}$ can be seen as a multiplex network [83,84] with layers representing time steps.

A. Static hidden-variables model

Here we describe the SHVM [18], which generates graphs by a two-step procedure. First, each node j (out of n total, labeled as $\{1, ..., n\} = [n]$) is assigned a *hidden variable* $h_j \in \mathcal{X}$, drawn independently with probability density $v(h_j)$ from set $\mathcal{X}$. Thus the hidden-variable configuration is $H = \{h_j\}_{j=1}^n \in \mathcal{H} = \mathcal{X}^n$ and the joint HV density is $\rho(H) = \prod_{j=1}^n v(h_j)$. Second, node pairs ij ($1 \leqslant i < j \leqslant n$) connect with pairwise probability $f(h_i, h_j)$, independently from one another. The conditional probability $\mathbb{P}(G|H)$ of a graph G is thus given by

$$\mathbb{P}(G|H) = \prod_{1 \leqslant i < j \leqslant n} (f(h_i, h_j))^{A_{ij}} (1 - f(h_i, h_j))^{1-A_{ij}}, \quad (5)$$

where $\{A_{ij}\}_{1 \leqslant i < j \leqslant n}$ are elements of the adjacency matrix of graph G. For a fixed H, this is an edge-independent random graph. But since H is random, $\mathbb{P}(G)$ is a probabilistic mixture of Eq. (5) over possible HV configurations $H \in \mathcal{X}^n$ via Eq. (1).

B. Temporal hidden-variables model

We now describe a temporal version of the SHVM (Sec. III A), namely, the TVHM. We denote by $A_{ij}^{(t)}$ the ijth element of $G^{(t)}$'s adjacency matrix. The initial conditions $(G^{(1)}, \{h_j^{(1)}\}_{j=1}^n)$ are sampled from the SHVM. For $t \in \{1, ..., T - 1\}$, the system updates according to:

(a) *HV dynamics.* Each node j samples $h_j^{(t+1)}$ from a conditional density $\mathcal{P}_h(h_j^{(t+1)}|h_j^{(t)})$, discussed below.

(b) *Link resampling.* Each node pair ij, with probability ω, resamples $A_{ij}^{(t+1)}$ with connection probability $f(h_i^{(t+1)}, h_j^{(t+1)})$. Otherwise, $A_{ij}^{(t+1)} = A_{ij}^{(t)}$.

Simply put, each node's HV undergoes Markovian dynamics (governed by $\mathcal{P}_h$), and each node-pair ij is re-evaluated for linking (with probability ω each time step) with connection probability equal to ij's current affinity value $f(h_i^{(t+1)}, h_j^{(t+1)})$. We separately consider two types of HV dynamics $\mathcal{P}_h$:

(a) *Jump dynamics.* Each node j, with probability $\sigma \in [0, 1]$, resamples its HV to obtain $h_j^{(t+1)}$. The conditional

density for jump dynamics is thus

$$\mathcal{P}_h(h'|h) = \sigma \nu(h') + (1 - \sigma)\mathbf{1}_h(h'), \qquad (6)$$

with $\mathbf{1}_h(h')$ being the Dirac measure.

(b) *Walk dynamics:* The HV of every node moves to a nearby point in $\mathcal{X}$ using Brownian-like motion with the average step length proportional to parameter $\sigma \in [0, 1]$.

We implement the latter option by transforming the density $\nu(h)$ on $\mathcal{X}$ to the uniform density on $[0, 1]^D$, where D is the dimension of $\mathcal{X}$, using the inverse cumulative distribution function (CDF) transform. We then do a random walk in $[0, 1]^D$, with step size proportional to σ, preserving the uniform distribution. Transformed back to $\mathcal{X}$, the random walk increments preserve the distribution $\nu(h)$. The details are in Appendix D.

In both walk dynamics and jump dynamics, parameter σ encodes the rate of change of HVs. Also, in both cases, the transition probability density $\mathcal{P}_H$ is separable due to independence of $\{h_j^{(t)}\}_{j=1}^n$:

$$\mathcal{P}_H(H^{(t+1)}|H^{(t)}) = \prod_{j=1}^{n} \mathcal{P}_h\left(h_j^{(t+1)}\big|h_j^{(t)}\right). \qquad (7)$$

The stationary density of the above dynamics is equal to the static-model HV density ρ. The density of $\mathbf{H} = \{\{h_j^{(t)}\}_{j=1}^n\}_{t=1}^T$ is also separable,

$$p(\mathbf{H}) = \prod_{j=1}^{n}\left(\nu\big(h_j^{(1)}\big)\prod_{t=1}^{T-1}\mathcal{P}_h\big(h_j^{(t+1)}\big|h_j^{(t)}\big)\right). \qquad (8)$$

The probability of a graph sequence $\mathbf{G}$ given $\mathbf{H}$ is the temporal product (3) of the following transition probabilities:

$$\mathcal{P}_G(G^{(t+1)}|G^{(t)}, H^{(t+1)}) = \prod_{1 \leqslant i < j \leqslant n} Y_{ij}^{A_{ij}^{(t+1)}}(1 - Y_{ij})^{1-A_{ij}^{(t+1)}}, \qquad (9)$$

with Y_{ij} denoting the conditional linking probability,

$$Y_{ij} = \omega f\big(h_i^{(t+1)}, h_j^{(t+1)}\big) + (1 - \omega)A_{ij}^{(t)}, \qquad (10)$$

encoding the fact that link resampling happens with probability ω, and that otherwise the link (or nonlink) remains the same.

We will primarily quantify the structure of THVM snapshots via the *effective connection probability*,

$$\bar{f}(h, h') = \lim_{t \to \infty} \mathbb{P}\big(A_{ij}^{(t)} = 1\big|h_i^{(t)} = h, h_j^{(t)} = h'\big), \qquad (11)$$

which, if the equilibrium property is satisfied, is the same as the affinity function $f(h, h')$. If the affinity is a function of a composite variable such as the distance between or the product of the pair of HVs, the effective connection probability is defined analogously but for those composite quantities. We note here that the average degree (number of link ends per node) is independent of the values of σ and ω in THVM snapshots (see Appendix A).

IV. PARAMETER SPACE AND RESULTING DYNAMICS OF TEMPORAL HIDDEN VARIABLE MODELS

In this section, we consider several limiting cases in the space of dynamics parameters $(\sigma, \omega) \in [0, 1]^2$, and some

special-case categories of affinity function f. The resulting regimes exhibit a variety of qualitatively distinct behaviors. If $\sigma = \omega = 0$, a single graph is sampled from the static model and all of its HVs and links are held fixed for all t. To the opposite extreme, if $\sigma = \omega = 1$, at each time step, every node's HV is fully randomized, and then all possible links are reevaluated, resulting in a sequence of i.i.d. instances of the static model. In either case, the equilibrium property is satisfied—but the persistence property is not for $\sigma = \omega = 1$ (there is no persistence), whereas for $\sigma = \omega = 0$ there is complete persistence.

In Secs. IV A–IV D, several other parameter regimes are analyzed. We discuss the behavior of temporal networks in each case, how well they qualify in terms of the equilibrium and persistence properties, and their relations to preexisting commonly studied static network ensembles. Table I shows the different special cases, while a schematic picture of the space of dynamics parameters is shown in Fig. 1.

A. Quasistatic regime ($\alpha_2(\sigma, \omega) \approx 1$)

Here we consider the parameter regime quantified by the condition $\alpha_2(\sigma, \omega) \approx 1$ (upper-left region of Fig. 1), where

$$\alpha_2(\sigma, \omega) = \frac{\omega}{1 - (1 - \omega)(1 - \sigma)^2} \in [0, 1], \qquad (12)$$

in which networks have both random link structure and random HVs, and exhibit both the persistence property and the equilibrium property. The quantity $\alpha_2(\sigma, \omega)$ is a naturally arising function characterizing how effective connection probabilities differ from their static-model counterparts (see Appendix A). The equilibrium property is satisfied due to sufficient timescale separation: link resampling happens quickly enough relative to HV motion for $G^{(t)}$ to remain caught up with $H^{(t)}$. The dynamics can thus be considered quasistatic in the sense of quasistatic transformations in classical equilibrium thermodynamics [85]. Over time, the HV configuration and link structure both fully explore their respective spaces, functioning as a temporal network whose stationary distribution is the SHVM defined in Sec. III A. Note that the equilibrium property is only *approximately* satisfied if $\alpha_2(\sigma, \omega) < 1$, that approximation becoming exact only in limit of extreme timescale separation or $\alpha_2(\sigma, \omega) = 1$. Two regimes at the boundary of the quasistatic regime have exact satisfaction of the equilibrium property: $\omega = 1$ (Sec. IV B) and $\sigma = 0$ (Sec. IV C). Adding a third mechanism of dynamics allows for exact satisfaction of the equilibrium property at all $(\sigma, \omega) \in [0, 1]^2$ (see Sec. VI).

B. Complete link resampling ($\omega = 1$)

Here we consider the case $\omega = 1$ (top region of Fig. 1). This case resembles that of the quasistatic regime, but all links form based on *current* HV configurations, so there is no graph-encoded memory: $\mathcal{P}_G(G^{(t+1)}|G^{(t)}, \mathbf{H}) = \mathbb{P}(G^{(t+1)}|H^{(t+1)})$. The resulting Markov chain on $\mathcal{H} \times \mathcal{G}$ thus satisfies the equilibrium property *exactly*, as opposed to approximately in the quasistatic regime (Sec. IV A). Link structure when $\omega = 1$ is more correlated over time than two i.i.d. samples from the SHVM (due to persistence in HV configurations) but the specific level of persistence depends on

TABLE I. Table of limiting cases of dynamics parameters (σ, ω) for THVMs. The first and second columns provide a short-hand name and the associated parameter regime. The third column states whether the equilibrium property is satisfied, whereas the fourth column states whether the persistence property is satisfied (in a way that is tunable at any desired level, which, for instance, leaves out the case $\sigma = \omega = 0$).

Name	Parameter regime	Equilibrium property	Tunable persistence
Single static graph	$\omega = \sigma = 0$	Yes	No
i.i.d. graph sequence	$\omega = \sigma = 1$	Yes	No
Quasistatic	$\alpha_2(\sigma, \omega) \approx 1$ [Eq. (12)]	Yes[a]	Yes
Complete link resampling	$\omega = 1, \sigma \in (0, 1)$	Yes	Depends on f[b]
Deterministic HV to graph	$\omega = 1, f : \mathcal{X}^2 \rightarrow \{0, 1\}$	Yes	Depends on f[b]
Complete HV resampling	$\sigma = 1, \omega \in (0, 1)$	No	Yes[c]
Fixed HVs	$\sigma = 0$	Yes	Yes
Erdős-Rényi-like	$\sigma/\omega \gg 1$	No	No
Fixed graph structure	$\omega = 0$	Yes[d]	No[d]

[a]In the quasistatic regime, $G^{(t)}$ will have arisen from an HV configuration closely resembling $H^{(t)}$, due to a timescale separation. This implies *approximate*, rather than exact, satisfaction of the equilibrium property.

[b]When $\omega = 1$, although the persistence property is in general lost due to each possible edge being resampled at every time step, there is still *some* persistence present, tuned by σ and dependent upon the affinity function f.

[c]When $\sigma = 1$, the persistence property is tunably satisfied at the level of graph structure but not at all at the level of hidden variables, which are completely resampled every time step.

[d]In the case of $\omega = 0$, the initial graph remains fixed for all time, while HVs change. Since the initial condition is sampled from the static model, this regime technically satisfies the equilibrium property. It does so both at the level of graphs and at the level of hidden variables but not at all at the *joint* level. Persistence is not tunable at the level of graphs but is at the level of hidden variables.

the form of the affinity function $f(h, h')$ and on σ. A variety of temporal network models have fully resampled edges at each time step [72,86,87].

As subset of the $\omega = 1$ regime, consider THVMs with binary affinity function $f : \mathcal{X}^2 \rightarrow \{0, 1\}$. In this case, *all randomness comes from HVs* because f deterministically maps HV configurations to graphs. The static model's conditional probability distribution in such cases is given by a product of indicator functions,

$$\mathbb{P}(G|H) = \prod_{1 \leqslant i < j \leqslant n} \mathbf{1}\{A_{ij} = f(h_i, h_j)\}, \qquad (13)$$

equal to 1 if and only if $f(h_i, h_j) = A_{ij}$ for all ij, and equal to zero otherwise. Since the HV dynamics $\mathcal{P}_H$ conserves ρ, and since $\omega = 1$ ensures that all node pairs have up-to-date links with respect to HVs, this model satisfies the equilibrium property *exactly*. The rate of HV dynamics, and thus of link dynamics, is controlled by σ (but also influenced by the form of f). This regime encompasses sharp RGGs of any kind [21]; see Sec. V B for temporal RGGs with $\omega \in [0, 1]$.

C. Fixed hidden variables ($\sigma = 0$)

Here we consider $\sigma = 0$ (left region of Fig. 1), in which case all HVs are frozen in place, ensuring satisfaction of the equilibrium property. The initial HV configuration $H^{(1)}$ has the SHVM density ρ, but conditioning on some particular initial configuration $H^{(1)}$ yields fixed pairwise connection probabilities $p_{ij} = f(h_i, h_j)$, resulting in temporal versions of edge-independent static networks [88–90]. Analytical expressions for link dynamics can be written straightforwardly in terms of the set of values $\{p_{ij}\}_{1 \leqslant i < j \leqslant n}$ and the parameter ω. The transition probability $\mathcal{P}_G(G^{(t+1)}|G^{(t)})$ is

$$\mathcal{P}_G(G^{(t+1)}|G^{(t)}) = \prod_{1 \leqslant i < j \leqslant n} p_{ij}^{A_{ij}^{(t)} \rightarrow A_{ij}^{(t+1)}}, \qquad (14)$$

where $p_{ij}^{0 \rightarrow 0}$, $p_{ij}^{0 \rightarrow 1}$, $p_{ij}^{1 \rightarrow 0}$, and $p_{ij}^{1 \rightarrow 1}$ are, respectively, the nonlink persistence, link-formation, link-removal, and link-persistence probabilities for node pair ij. That is, $p_{ij}^{\alpha \rightarrow \beta} = \mathbb{P}(A_{ij}^{(t+1)} = \beta | A_{ij}^{(t)} = \alpha)$, given by

$$p_{ij}^{\alpha \rightarrow \beta} = (1 - \omega p_{ij})^{(1-\alpha)(1-\beta)} (\omega p_{ij})^{(1-\alpha)\beta}$$
$$\times (\omega(1 - p_{ij}))^{\alpha(1-\beta)} (1 - \omega(1 - p_{ij}))^{\alpha\beta}. \quad (15)$$

Many static network models have independent edges with predefined connection probabilities and thus can be made temporal as THVMs with $\sigma = 0$. Examples include the Erdős-Rényi (ER) model [91] the (soft) SBM [92], and inhomogeneous random graphs [88] with fixed coordinates.

The persistence property can be quantified by any of the numerous measures of graph dissimilarity [80] by application to graph pairs at neighboring time steps. A simple example in the $\sigma = 0$ setting is the expected Hamming dissimilarity [93],

$$\sum_{1 \leqslant i < j \leqslant n} \mathbb{P}(A_{ij}^{(t)} \neq A_{ij}^{(t+1)})$$
$$= \sum_{1 \leqslant i < j \leqslant n} (p_{ij}^{1 \rightarrow 0} p_{ij} + p_{ij}^{0 \rightarrow 1}(1 - p_{ij}))$$
$$= 2\omega \sum_{1 \leqslant i < j \leqslant n} p_{ij}(1 - p_{ij}), \qquad (16)$$

which simplifies substantially in some cases, for instance, the ER model ($p_{ij} = p$ for all ij), leaving $2\omega p(1 - p)\binom{n}{2}$. The parameter ω directly tunes the level of persistence, with $\omega = 0$ yielding the highest persistence (an unchanging graph) and $\omega = 1$ yielding the lowest persistence (a fully resampled graph).

Edge-resampling dynamics with fixed p_{ij} values closely resembles *dynamic percolation* [94], which has been investigated in lattices [95], trees [96], and ER graphs [97,98], and also relates to *edge-Markovian networks* [99–101].
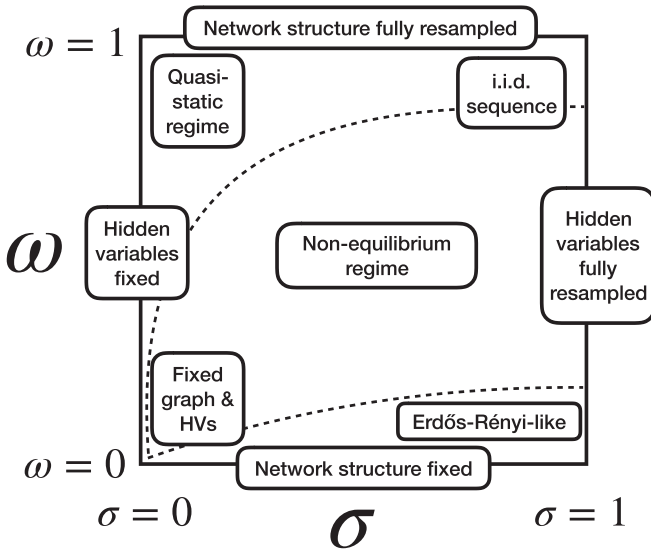
FIG. 1. Two-parameter space of possible dynamics. The two parameters $(\sigma, \omega) \in [0, 1]^2$ tune the rate of change of hidden variables and rate of resampling of links, respectively. In general, with dynamic hidden variables, link-structure is out of equilibrium relative to the configuration of hidden variables at any particular time step, violating the equilibrium property. In the quasistatic regime (upper left) and along the upper and leftward boundary regions ($\omega = 1$ and $\sigma = 0$, respectively), the equilibrium property is recovered. In the lower-right regime, HVs are so randomized that network snapshots resemble Erdős-Rényi graphs. At $\sigma = 1$ (right-hand boundary), all hidden variables are resampled at every time step, but only a fraction ω of links resampled. If $\omega = 0$ (lower boundary), the network structure remains fixed for all time, regardless of the hidden-variable dynamics. The dashed curves distinguish, qualitatively, three regimes: the quasistatic regime lies above the upper dashed curve, the Erdős-Rényi-like regime lies below the lower dashed curve, and the general nonequilibrium regime lies in between. The shapes of the dashed curves come from contours of the function $\alpha_2(\sigma, \omega)$: the upper curve approximately designates $\alpha_2(\sigma, \omega) = 0.85$, whereas the lower curve approximately designates $\alpha_2(\sigma, \omega) = 0.15$ (see Sec. IV A and Fig. 3). Both curves emanate from (0,0) and reach the $\sigma = 1$ boundary at the values of $\alpha_2(1, \omega) = \omega \approx 0.85$ (upper curve) and $\alpha_2(1, \omega) = \omega \approx 0.15$ (lower curve), see Eq. (12).

D. Complete resampling of hidden variables ($\sigma = 1$)

Here we consider the case for which all HVs are resampled at every time step ($\sigma = 1$), so no HV-driven structural persistence exists (right region of Fig. 1). Note that walk dynamics is parameterized by σ so $\sigma = 1$ implies complete HV randomization. If $\sigma = 1$, correlations among links (and nonlinks) do still exist due to simultaneous resampling; the set of node pairs selected for link resampling at time step t forms links based upon the *same* underlying HV configuration $H^{(t)}$. In this setting, ω quantifies the level of agreement among node pairs as to what the HV configuration is. For instance, in spatial network models, if $\sigma = 1$, then ω directly controls the level of geometry-induced correlations.

Given the HV configuration at time t and averaging over all past time steps, node pair ij is connected with probability

$$\mathbb{P}\left(A_{ij}^{(t)} = 1 \big| h_i^{(t)}, h_j^{(t)}\right) = \omega f\left(h_i^{(t)}, h_j^{(t)}\right) + (1 - \omega)\langle f \rangle, \quad (17)$$

where $\langle f \rangle = \int_{\mathcal{X}^2} \nu(h)\nu(h')f(h, h')dh dh'$ is the expected affinity of a pair of nodes with randomized HVs. The expression 17 is an example of an effective connection probability which deviates from the static-model affinity function. A more general formula for the effective connection probability in the case of jump dynamics and arbitrary $f(h, h')$, σ, and ω is derived in Appendix A, and some special cases are described in the examples in Secs. V A–V D. As $\omega \to 0$ with $\sigma = 1$ (and in general for $\sigma/\omega \gg 1$), the model approaches a temporal version of the ER model, since each node pair at the time of link resampling will have completely randomized HVs; each edge will then independently exist with probability $\langle f \rangle$ if $0 < \omega \ll 1$. If $\omega = 0$, we have a fixed graph structure, i.e., a network that simply remains as whatever the initially sampled graph was, but with dynamic HVs (for any $\sigma > 0$).

V. TEMPORAL EXTENSIONS OF POPULAR STATIC NETWORK MODELS

This section contains several examples of THVMs. In each subsection, we describe a SHVM, its temporal extension according to the modeling framework of Sec. III B, and the effective connection probability that arises due to the dynamics, and offer some additional discussion. We specifically consider temporal extensions of the following static network models: SBMs [20], RGGs [21], hypersoft configuration models (HSCMs) [22], and hyperbolic graphs [15].

A. Temporal stochastic block models

This subsection considers temporal extensions of SBMs, which are used to model community structure in networks [20,92,102,103].

1. Static hyperparametric SBMs

We consider a static network with conditionally Bernoulli-distributed edges amongst n nodes $j \in [n]$, each node having been randomly assigned to one of m groups (a.k.a. communities, blocks, colors). Each node j independently draws a group index $q_j \in [m] = \{1, ..., m\}$ from probability distribution $\varrho = \{\varrho_q\}_{q \in [m]}$. Each node pair then connects with probability f_{q_i, q_j}. In this definition, the group memberships $\{q_j\}_{j \in [n]}$ are not externally specified as model parameters—rather, their distribution ϱ is specified. Thus, the group memberships are hyperparameters, and we refer to these static networks as hyperparameteric SBMs or hyper-SBMs (equivalent to inhomogeneous random graphs with hidden color [105,106]). The expected number of nodes n_q in a given block q is $\langle n_q \rangle = n\varrho_q$, and the joint distribution of $\{n_q\}_{q \in [m]}$ is multinomial. Note that this model could be formulated with continuous HVs as per Sec. III A, but we instead use discrete HVs for simplicity (see Appendix H for the continuous-to-discrete mapping). As an illustrative example to be used throughout this section, we consider the case of $m = 2$ groups, with $\varrho_1 = 1 - \varrho_2 = u$. The within-group affinity is $p = f_{1,1} = f_{2,2}$, and the between-group affinity is zero ($f_{1,2} = 0$).

2. Temporal hyper-SBMs

To make the hyper-SBM dynamic, at each time step $t \in \{2, ..., T\}$ each node i with probability σ resamples its group
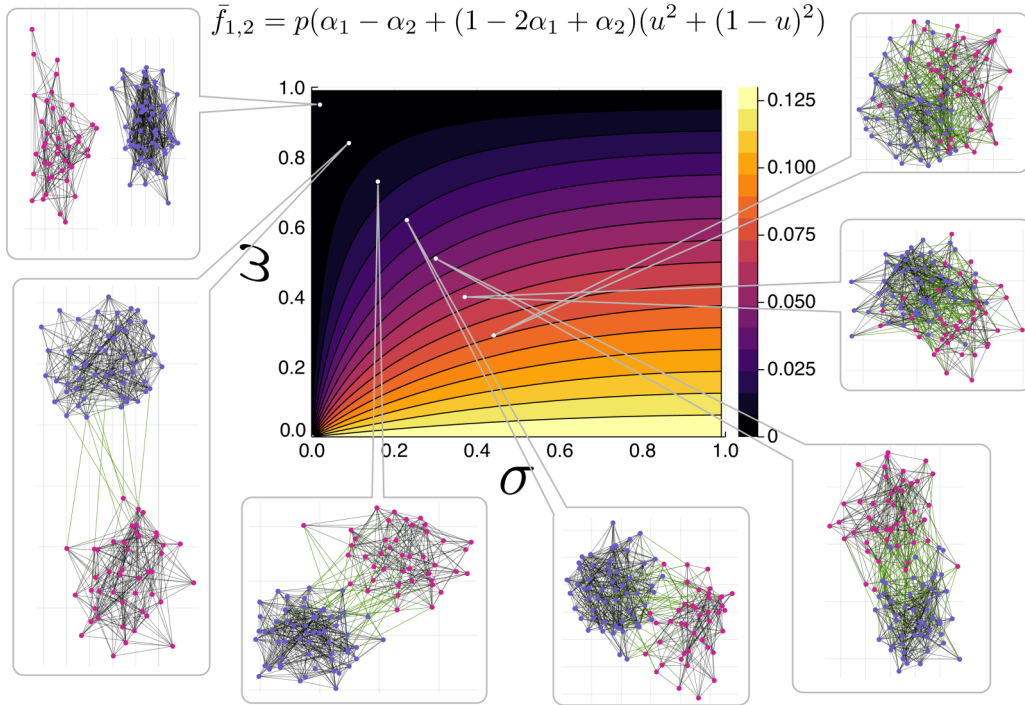
FIG. 2. Snapshots of a temporal stochastic block model: A modular network with dynamic group assignments and link resampling. The $n = 100$ nodes are partitioned into two groups with group-membership probabilities $\varrho_1 = 0.4 = 1 - \varrho_2$, and group memberships change in time by group resampling with probability σ. The affinity function is $f_{q,q'} = p\mathbf{1}\{q = q'\}$ with $p = 0.25$, disallowing intergroup connections in the *static* model. Network snapshots are displayed via a spring-force layout algorithm [104], for various parameters (σ, ω) such that networks span a variety of structural outcomes. Node coloration is by group membership and link coloration is black for within-group links and green for between-group links. In the central panel, the effective connection probability $\bar{f}_{1,2}$ between communities is plotted. Outside of the quasistatic regime, group-membership dynamics is fast enough for a substantial number of intergroup links to exist ($\bar{f}_{1,2} > 0$), despite the intergroup connection *formation* probability being $f_{1,2} = 0$.

index $q_i^{(t)}$ from distribution ϱ, and then each node pair ij with probability ω resamples $A_{ij}^{(t)}$ with connection probability $f_{q_i^{(t)}, q_j^{(t)}}$. Thus,

$$\mathbb{P}\left(q_i^{(t)} = q' \big| q_i^{(t-1)} = q\right) = (1 - \sigma)\mathbf{1}\{q = q'\} + \sigma\varrho_{q'} \quad (18)$$

and

$$\mathbb{P}\left(A_{ij}^{(t)} = 1 \big| A_{ij}^{(t-1)}, q_i^{(t)}, q_j^{(t)}\right) = (1 - \omega)A_{ij}^{(t-1)} + \omega f_{q_i^{(t)}, q_j^{(t)}}. \tag{19}$$

See Fig. 2 for visualized embeddings of network snapshots from the stationary distribution of the example $m = 2$, $\varrho_1 = u = 1 - \varrho_2$, $f_{q,q'} = p\mathbf{1}\{q = q'\}$.

3. Effective connection probabilities in hyper-SBMs

The block dynamics of nodes in temporal hyper-SBMs introduces several novel features to the system. First, pairwise affinities change over time. Second, the set of all existing links at time t need not have arisen from the group assignments of time t. Temporal snapshots in general thus deviate from the static model—the equilibrium property does not necessarily hold. However, even if snapshots do not resemble *the* static model, they do resemble *a* static model—an *effective* SBM. Consider two nodes, with current group indices q, q'. Averaging over all past values of HVs, we obtain the effective connection probability $\bar{f}_{q,q'}$ for dynamic hyper-SBMs. Since the SBM case is directly obtainable from discretization of the

continuous model (see Appendix H), we can use a discrete version of the general formula derived in Appendix A, namely,

$$\begin{aligned} \bar{f}_{q,q'} = {} & \alpha_2 f_{q,q'} \\ & + (\alpha_1 - \alpha_2)(\langle f_{q,\cdot}\rangle + \langle f_{q',\cdot}\rangle) \\ & + (1 - 2\alpha_1 + \alpha_2)\langle f\rangle, \end{aligned} \tag{20}$$

where coefficients $\alpha_b(\sigma, \omega)$ for $b \in \{1, 2\}$ are given by

$$\alpha_b = \frac{\omega}{1 - (1 - \omega)(1 - \sigma)^b}, \tag{21}$$

and marginally averaged affinities are

$$\begin{aligned} \langle f_{q,\cdot}\rangle &= \sum_{q'} \varrho_{q'} f_{q,q'}, \\ \langle f\rangle &= \sum_q \varrho_q \langle f_{q,\cdot}\rangle = \sum_{q,q'} \varrho_q \varrho_{q'} f_{q,q'}. \end{aligned} \tag{22}$$

Note that when $\sigma = 1$ we have $\alpha_1(1, \omega) = \alpha_2(1, \omega) = \omega$ and Eq. (20) reduces to the form of Eq. (17). In the simple example case ($m = 2$, $\varrho_1 = u$, $f_{q,q'} = p\mathbf{1}\{q = q'\}$), terms in $\bar{f}_{q,q'}$ are evaluated as

$$\begin{aligned} \langle f_{1,\cdot}\rangle &= up, \\ \langle f_{2,\cdot}\rangle &= (1 - u)p, \\ \langle f\rangle &= p(u^2 + (1 - u)^2), \end{aligned} \tag{23}$$

from which the formula for $\bar{f}_{q,q'}$ becomes

$$\bar{f}_{q,q'} = \alpha_2 p \mathbf{1}\{q = q'\}$$
$$+ (\alpha_1 - \alpha_2) \begin{cases} 2up, & q = q' = 1 \\ 2(1-u)p, & q = q' = 2 \\ p & q \neq q' \end{cases}$$
$$+ (1 - 2\alpha_1 + \alpha_2)p(u^2 + (1-u)^2). \qquad (24)$$

In particular, the between-group effective connection probability becomes

$$\bar{f}_{1,2} = p(\alpha_1 - \alpha_2 + (1 - 2\alpha_1 + \alpha_2)(u^2 + (1-u)^2)), \quad (25)$$

which is visualized in Fig. 2. In the extreme case of $\sigma/\omega \gg 1$, all links form between nodes with effectively random group assignments, making all pairs equally likely to connect, and reducing the system to a temporal ER network of connection probability $p(u^2 + (1-u)^2)$.

4. Temporal hyper-SBM discussion

Interesting examples of qualitative realism arise in temporal hyper-SBMs. For instance, group dynamics of nodes yields intergroup connectivity, as is observed in real systems. If someone joins a different club, switches political parties, or emigrates to a new country, they at first primarily carry ties to their original group—and thus upon changing group membership, they suddenly have many intergroup links—*not* because of intergroup link formation, but because of dynamic group membership. Likewise, within-group connectivity can be *lower* than in the static model, as is the case in real systems due to nodes having recently arrived from another group or from neighbor nodes having recently departed. These effects arise *outside* the quasistatic regime, so we speculate that in some cases the *nonequilibrium* regime can better emulate real-world systems. We also note that we here considered group-resampling HV-dynamics (a discrete version of jump dynamics), but we could also consider a general Markov chain on group assignments with stationary distribution ϱ.

B. Temporal random geometric graphs

In this section, we describe THVMs arising from static RGGs, which model the influence of an underlying geometry on graph structure [21].

1. Static random geometric graphs

In RGGs, nodes are assigned spatial coordinates as HVs, and node pairs are linked if their coordinates are closer than some threshold distance r. Hence the affinity is binary, $f(h_i, h_j) = \mathbf{1}\{d_{\mathcal{X}}(h_i, h_j) \leqslant r\}$, with $d_{\mathcal{X}} : \mathcal{X}^2 \to [0, \infty)$ denoting the geodesic distance in latent space $\mathcal{X}$. Examples of well-studied RGGs include Euclidean RGGs with periodic or nonperiodic boundary conditions [21], spherical RGGs [107], and hyperbolic RGGs (the hyperbolic model with inverse-temperature parameter $\beta = \infty$ [15]). As a primary example, we consider a simple one-dimensional RGG with periodic boundary conditions: $\mathcal{X} = [0, 1]$ and $d_{\mathcal{X}}(h_i, h_j) = 1/2 - |1/2 - |h_i - h_j||$.

2. Temporal RGGs

To go from static RGGs to temporal RGGs, we incorporate coordinate dynamics and link-resampling dynamics. We consider here jump dynamics, each node resampling its coordinate according to the static-model density ν, with probability σ, each time step $t \in \{2, ..., T\}$ (the coordinate density follows Eq. (6), with $\nu(h) = 1$ for the uniform density on the unit interval). Link resampling happens independently for each node pair with probability ω each time step. Since RGGs have deterministic connectivity, link resampling of ij at time t guarantees that $A_{ij}^{(t)} = 1$ if $d_{\mathcal{X}}(h_i^{(t)}, h_j^{(t)}) \leqslant r$ and $A_{ij}^{(t)} = 0$ otherwise. But if ij's connectivity is not resampled at time t, links may fall out of equilibrium with respect to coordinates. Note that we could also study temporal RGGs with walk dynamics, with either periodic or reflecting boundary conditions; for simplicity, we study jump dynamics here, leaving temporal RGGs with walk dynamics for a future study.

3. Effective connection probabilities in temporal RGGs

We now describe the effective connection probability $\bar{f}(x)$ for RGGs between pairs of nodes for arbitrary (σ, ω). The expression for $\bar{f}(x)$ in temporal RGGs is derived in Appendix B, and the result is provided here:

$$\bar{f}(x) = \alpha_2 \mathbf{1}\{x \leqslant r\} + 2r(1 - \alpha_2). \qquad (26)$$

The quantity $\alpha_2 = \alpha_2(\sigma, \omega)$, defined in Eq. (21), directly governs the level of locality in temporal RGGs. See Fig. 3 for a visualization of the function $\alpha_2(\sigma, \omega)$ and of network snapshots across a range of (σ, ω)-values. The effective connection probability $\bar{f}(x)$ has a steplike form, with connection probability $\alpha_2 + 2r(1 - \alpha_2)$ for all $x \leqslant r$ and $2r(1 - \alpha_2)$ for all $x > r$. The above effective connection probability agrees perfectly with the results of numerical simulations, see Fig. 4.

4. Temporal RGG discussion

The naturally arising function $\alpha_2(\sigma, \omega) \in [0, 1]$ describes the level of locality in network snapshots (see Fig. 3), and quantifies the equilibrium property. It interpolates between the case of RGGs ($\alpha_2(\sigma, \omega) = 1$) and ER graphs ($\alpha_2(\sigma, \omega) = 0$), resembling the structural transition of the Watts-Strogatz model [108]. In this case, all links *form* locally and it is dynamics of *node positions* that induces the transition (alongside the formation of local links at the nodes' new locations); a similar phenomenon has been observed in contagion dynamics among mobile agents [109]. Also note, in dynamic RGGs, links can exist that were not *possible* in the static model model: links of length greater than r, since the effective connection probability $\bar{f}(x)$ no longer goes completely to zero for $x > r$ [see Eq. (26)]. This is related to phenomena observed in real-world networks: pairs of people may form friendships locally but maintain those friendships after becoming geographically separated, resulting in the existence of long-ranged social ties that would not likely have *formed* at that distance. Likewise, the function $\bar{f}(x)$ is also *less than one* for distances $x \leqslant r$, allowing for *nonlinks* that would be impossible in the static model. That phenomenon also appears in real-world systems: instead of individuals knowing everyone in their local vicinity, nonlinks between close-by pairs may exist due to them having only recently become proximate.
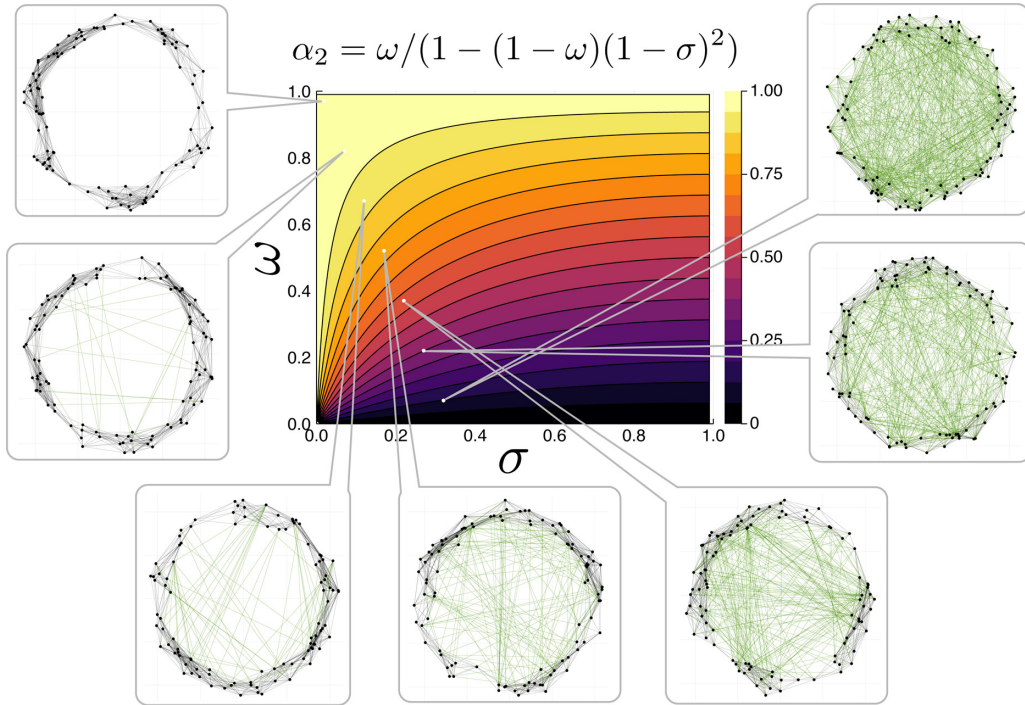
FIG. 3. Snapshots of a temporal random geometric graph: A geometrically embedded network with dynamic node coordinates and link resampling. Coordinates of $n = 100$ nodes are sprinkled uniformly into a 1D ring of unit circumference and change in time via jump dynamics (coordinate resampling with probability σ). The affinity as a function of distance is $f(x) = \mathbf{1}\{x \leqslant r\}$, where $r = 0.1$ is the connection radius, disallowing long-ranged links in the *static* model. Snapshots are shown at various values of (σ, ω), with the displayed embedding having angular positions equal to 2π times spatial coordinates and radial positions set equal to 1 plus some added random noise to aid with visualization of network connectivity among close by node pairs. Link coloration is according to length: black links are of distances $x \leqslant r$ whereas green links are of distances $x > r$. In the central panel, the function $\alpha_2(\sigma, \omega) \in [0, 1]$ is visualized, which encodes the level of locality in temporal RGGs [see Eq. (26)].

As with the case of temporal hyper-SBMs, these examples of qualitative realism are *in conflict* with the equilibrium property. Note also that similar deviations of $\bar{f}(x)$ relative to

FIG. 4. The effective connection probability, in theory and simulation, for 1D RGGs at various values of the dynamics parameters (σ, ω). The static model affinity function $f(x)$ is plotted with square markers. The solid lines are numerical estimates of the effective connection probability $\bar{f}(x)$ (with ω increasing as colors change from blue to yellow), whereas the dotted lines are the theoretical effective connection probability [Eq. (26)].

$f(x)$ occur in THVMs arising from *soft* RGGs, [110–113], for example, the $\mathbb{H}^2$ model (see Sec. V D).

C. Temporal hypersoft configuration model

In this section, we consider a dynamic version of HSCMs, which model networks with degree heterogeneity [22].

1. Static hypersoft configuration model

The static model we now consider is the HSCM [22,114], a hyperparametric version of an SCM. SCMs come in several varieties such as the Chung-Lu model [115], inhomogeneous random graphs [88], and the Norros-Reittu model [116]. Node pairs connect with A_{ij} values being independent (typically Bernoulli or Poisson distributed), such that, on average, each node has a particular degree value. In hyperparametric SCMs, that degree value is randomly assigned, according to some specified distribution of expected degrees. For example, one way to obtain SCMs with a degree distribution that is Pareto-mixed Poisson (with, say, power-law tail exponent γ and expected degree $\langle k \rangle$), is for nodes $j \in [n]$ to be assigned HVs $h_j \in [h_-, \infty)$ drawn from a Pareto density $v(h) = (\gamma - 1)h_-^{\gamma-1}h^{-\gamma}$, with minimal HV value $h_- = (\gamma - 2)\langle k \rangle/(\gamma - 1)$, and then for node pairs to be connected with probability

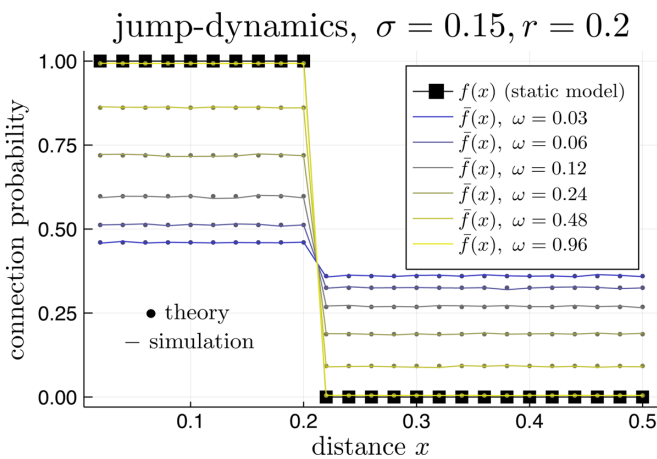$$f(h_i, h_j) = \frac{1}{1 + n\langle k \rangle/h_i h_j} \approx \frac{h_i h_j}{n\langle k \rangle}, \qquad (27)$$

degree evolution, $\langle k_j^{(t)} | \{ h_j^{(t-s)} \}_{s \geq 0} \rangle$
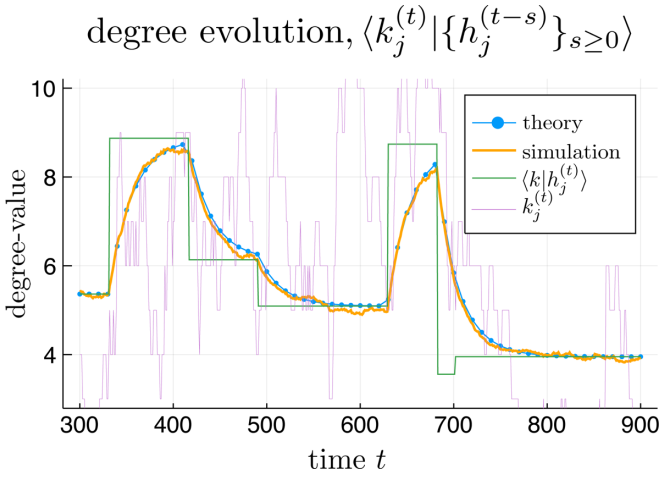

FIG. 5. Expected degree over time of a node in a temporal hypersoft configuration model with jump dynamics of hidden variables. Each node's expected degree (blue dotted curve) equilibrates toward its current static-model expected degree (green solid curve), as per Eq. (29). In any realization, the *actual* degree over time fluctuates (purple curve) but its ensemble average (orange solid curve) behaves as predicted. The average was obtained by simulating 1000 realizations with $(n, \langle k \rangle, \gamma, \omega, \sigma) = (200, 8, 2.8, 0.04, 0.01)$, keeping the HV trajectory $\{ h_j^{(t)} \}_{t=1}^T$ of a single node j fixed across trials.

the approximation holding when $h_i h_j / n \langle k \rangle \ll 1$. The expected degree of a node i in the static model is

$$\langle k_i | h_i \rangle = (n-1) \int_{h_-}^{\infty} f(h_i, h) \nu(h) dh \approx h_i. \quad (28)$$

The *actual* degrees of nodes are sharply peaked around their expected degrees, and thus the above implies that the degree distribution itself likewise has a power-law tail with exponent γ and mean $\langle k \rangle$.

2. Temporal HSCMs

Now we consider a temporal version of HSCMs. At each time step, each node j, with probability σ, resamples its HV $h_j^{(t)}$ from the static-model HV-density ν (jump dynamics). Then, each node pair ij ($1 \leq i < j \leq n$), with probability ω, has its indicator variable $A_{ij}^{(t)}$ resampled from a Bernoulli of mean $f(h_i^{(t)}, h_j^{(t)})$.

In the static model, the HV value h_j alone determines the expected degree $\langle k_j | h_j \rangle$. But in the temporal version, the quantity $h_i^{(t)}$ is time evolving, and the expected degree dynamically trails behind the static-model expected degree, equilibrating at a geometric pace (see Fig. 5):

$$\mathbb{E}\left[k_i^{(t)} \big| \{ h_i^{(t-s)} \}_{s \geq 0} \right]$$
$$= (n-1)\omega \sum_{s \geq 0} (1-\omega)^s \int_{h_-}^{\infty} f(h_i^{(t-s)}, h) \nu(h) dh$$
$$= \omega \sum_{s \geq 0} (1-\omega)^s \langle k_i | h_i^{(t-s)} \rangle. \quad (29)$$

We can also average the above over all HV values at time steps earlier than t, to obtain an *effective expected degree* that

depends only on $h_j^{(t)}$. To do this, we use the probability density of $h_j^{(t-s)}$ given $h_j^{(t)}$ under jump dynamics:

$$P_s\left(x | h_j^{(t)} \right) = (1-\sigma)^s \mathbf{1}_{h_j^{(t)}}(x) + (1 - (1-\sigma)^s)\nu(x). \quad (30)$$

Averaging Eq. (29) over HVs at all time steps $t - s$ for $s > 0$,

$$\mathbb{E}\left[k_i^{(t)} \big| h_i^{(t)} \right] = \omega \sum_{s \geq 0} (1-\omega)^s \int_{h_-}^{\infty} P_s\left(x | h_i^{(t)} \right) \langle k_i | x \rangle dx$$
$$= \alpha_1 \langle k_i | h_i^{(t)} \rangle + (1 - \alpha_1) \langle k \rangle, \quad (31)$$

where $\alpha_1(\sigma, \omega) = \omega / (1 - (1-\omega)(1-\sigma))$. In this case, α_1 measures the level of equilibration of node neighborhoods to their expected sizes. Having $\alpha_1 \approx 1$ indicates the quasistatic regime whereas $\alpha_1 \approx 0$ indicates an averaged-out behavior so the expected degree of any given node is simply the expected average degree $\langle k \rangle$ of the network.

3. Effective connection probabilities in temporal HSCMs

We now discuss effective connection probabilities in HSCMs. The formula derived in Appendix A applies, but note that the affinity $f(h, h')$ [Eq. (27)] is a function only of the product $\psi = hh'$. Thus we can examine the *effective connection probability* as a function of ψ, denoted $\bar{f}(\psi)$. To calculate $\bar{f}(\psi)$, we first must compute the probability density of a product of HVs in past time steps, given the value of the product at the current time step. We then sum the expected affinity given the product, weighted by $p_s = \omega(1-\omega)^s$, over all past time steps $s > 0$. These calculations require a variety of intermediate steps and are described in Appendix C.

4. Temporal HSCM discussion

Note that in HSCMs, nonequilibrium dynamics *reduces* degree heterogeneity; nodes with large HV values only transiently retain them. Equilibration, on the other hand, allows for a full structural expression of the nodes' internal heterogeneity. This implies that extremely heterogeneous real-world networks, if described by these models, would typically be in the quasistatic regime. We only considered jump dynamics here (resampling of static-model expected degree values) but we could alternatively study walk dynamics, where the nodes' HVs undergo a Brownian-like motion in a way that preserves ν. This could be achieved straightforwardly as described in Appendix D, alongside reflecting boundaries as studied in Appendix E.

D. Temporal hyperbolic graphs

In this section, we consider a temporal extension of the hyperbolic model [15] (the $\mathbb{H}^2$ model, for short), a geometry-based network model simultaneously exhibiting sparsity, clustering, small worldness [117,118], degree heterogeneity, community structure [119], and renormalizability [120].

1. Static $\mathbb{H}^2$ model

The $\mathbb{H}^2$ model is parameterized by a number of nodes n, average degree $\langle k \rangle$, power-law exponent γ, and inverse temperature β (which tunes the level of clustering). Hidden variables are polar coordinates, $h_j = (\theta_j, r_j)$, namely, a radial
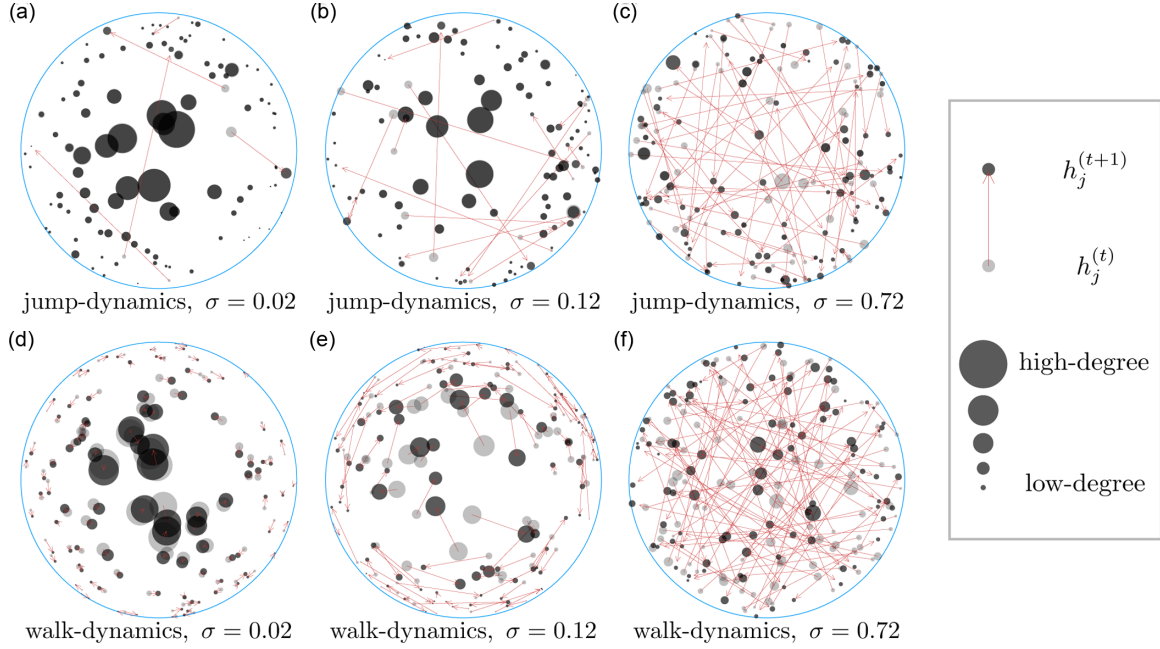
FIG. 6. Hidden-variable dynamics of nodes in a temporal $\mathbb{H}^2$ model, at increasing values of σ, with fixed $\omega = 0.1$. In each subplot, node coordinates for 100 random nodes are shown at two adjacent time steps, from a network with parameters $(n, \gamma, \beta, R) = (500, 2.2, 5, 8)$. Each arrow points from the coordinate location of a node at a given time step (grey) to the coordinate location of the same node at the next time step (black). (a)–(c) depict jump dynamics (coordinate resampling with probability σ, otherwise remaining in place), whereas (d)–(f) depict walk dynamics (all nodes move to neighboring locations, with mean step length parameterized by σ). Marker sizes are proportional to node degree values. For small σ/ω (a), (d), nodes' existing connections have arisen from approximately the present coordinates, making snapshots closely resemble the static hyperbolic model, as seen, e.g., by the exhibited degree heterogeneity. For larger σ/ω [(b), (e)], connections have arisen via mixtures of past and present coordinates, reducing degree heterogeneity. For very large σ/ω [(c), (f)], the system behaves similarly to a temporal Erdős-Rényi network.

coordinate $r_j \in [0, R]$ encoding the *popularity* of node j and an angular coordinate $\theta_j \in [0, 2\pi)$, encoding the *similarity* of node j to other nodes. These coordinates are sampled according to separable density $v(\theta, r) = v_{\text{ang}}(\theta) v_{\text{rad}}(r)$ where angles are distributed uniformly ($v_{\text{ang}}(\theta) = 1/2\pi$) and radii have an exponentially growing density,

$$v_{\text{rad}}(r) = \frac{\gamma - 1}{2} \frac{\sinh(\frac{\gamma-1}{2}r)}{\cosh(\frac{\gamma-1}{2}R) - 1}, \quad (32)$$

where $R = R(n, \langle k \rangle, \beta, \gamma)$ is selected so the mean degree is $\langle k \rangle$. The static-model affinity of node pair ij is a Fermi-Dirac function [121] (a sigmoid) of the hyperbolic geodesic distance x_{ij} between i and j,

$$f(h_i, h_j) = f(x_{ij}) = 1/(1 + e^{(\beta/2)(x_{ij} - R)}), \quad (33)$$

where $x_{ij} = x_{ij}(h_i, h_j)$ is given by

$$\cosh(x_{ij}) = \cosh(r_i)\cosh(r_j) \\ - \sinh(r_i)\sinh(r_j)\cos(\theta_{ij}), \quad (34)$$

with $\theta_{ij} = \pi - |\pi - |\theta_i - \theta_j||$. The connection probability and coordinate density in this model result in power-law degree distributions (but could also give rise to other degree distributions if the radial coordinate density was different), a similar feature to that exhibited by HSCMs—but also, the geometry arising from inclusion of the angular coordinate yields a large clustering coefficient and spatially localized link structure, making this model also similar to standard

RGGs. Increasing the parameter β yields a more localized link structure, approaching a step function as $\beta \to \infty$, leaving in that case an RGG (see Sec. V B 1) on the hyperbolic disk. As $\beta \to 0$, typical link lengths approach the system size and the model behaves similarly to the HSCM (see Sec. V C 1).

2. Temporal $\mathbb{H}^2$ model

To temporally extend the $\mathbb{H}^2$ model, we allow coordinate dynamics so each node j exhibits a trajectory in the hyperbolic disk, $h_j^{(t)} = (\theta_j^{(t)}, r_j^{(t)})$ for $t \in [T]$. For jump dynamics, each node jumps to a random location according to density $v(\theta, r)$, with probability σ each time step. For walk dynamics, each node j steps to a random location $h_j^{(t+1)}$ having angular and radial coordinates adjusted to relatively close-by values, with increasingly large steps for larger σ values; we describe the details of $\mathbb{H}^2$ walk dynamics in Appendix F. Dynamics of nodes on the hyperbolic disk is visualized in Fig. 6, for both jump dynamics and walk dynamics. For $\sigma \ll 1$, nodes rarely resample their coordinates (in jump dynamics) and step to only very localized regions (in walk dynamics). On the other hand, for $\sigma \approx 1$, almost all nodes resample their coordinates at each time step (in jump dynamics) or move to a nearly randomized location (in walk dynamics). We note that many other natural and interesting choices for HV dynamics exist, as we discuss in Sec. VIII and Appendix F.
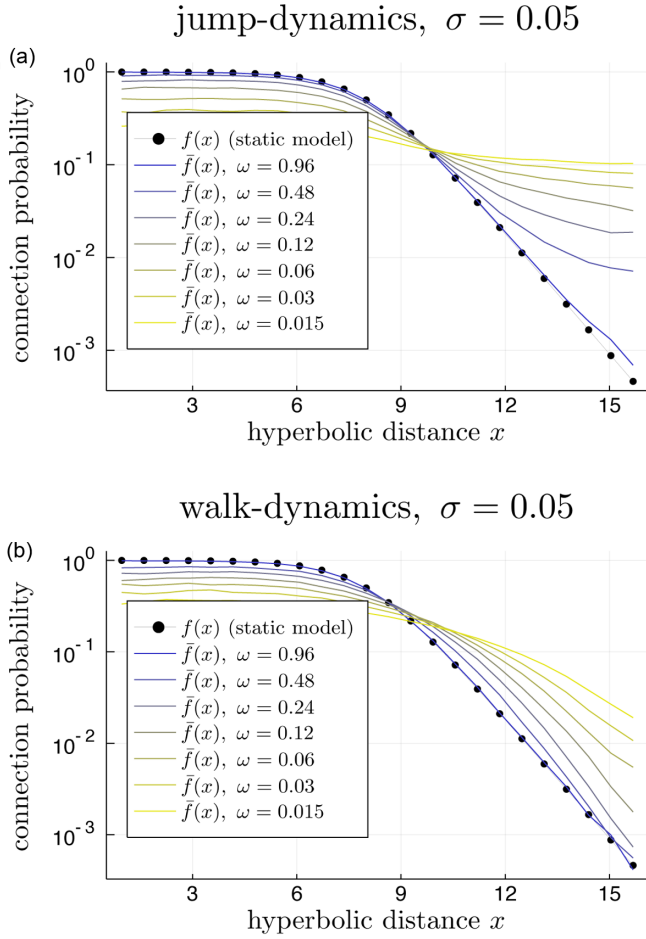
jump-dynamics, $\sigma = 0.05$

(a)

walk-dynamics, $\sigma = 0.05$

(b)

FIG. 7. Effective connection probability function $\bar{f}(x)$ in snapshots of a temporal hyperbolic model with $(n, \gamma, \beta, R) = (500, 2.2, 5, 8)$, for various values of ω. With slower link resampling (smaller ω), links are increasingly allowed to dynamically stretch before being removed by link resampling, resulting in deviations from the static-model affinity $f(x)$ (black dotted line). Coloration of the curve $\bar{f}(x)$ is from yellow to blue as ω increases. The upper panel, (a), shows the case of jump dynamics of coordinates. The lower panel, (b), shows the case of walk dynamics of coordinates. The choice of coordinate dynamics is consequential in the nonequilibrium regime, despite each having the same stationary density.

3. Effective connection probabilities in the temporal $\mathbb{H}^2$ model

In the temporal $\mathbb{H}^2$ model considered here, the effective connection probability $\bar{f}(x)$ no longer remains in the standard Fermi-Dirac form of $f(x)$ (see Fig. 7). With decreasing ω/σ, the connection probability function smooths out and extends to a longer range due to links being stretched more rapidly (for walk dynamics) or more frequently (for jump dynamics). This effect is more uniform and extends all the way out to long ranges for jump dynamics, whereas it is more localized for walk dynamics, for any given nonequilibrium value of (σ, ω).

Since the coordinates of $\mathbb{H}^2$ reflect popularity and similarity attributes, the effective connection probability and other nonequilibrium effects arising when outside of the quasistatic regime have specific interpretations. The set of current links arose from nodes having been connected at past time steps

when their previous similarity attributes were compatible (small hyperbolic distance); in real networks, such links may persist into the future even if the similarity attributes change. For instance, with social networks, consider friendships on Facebook, followers on Twitter, or author collaborations: similarity between connected pairs may decrease over time, but they tend to remain connected. Likewise, it could take some time for two people that become more similar to discover one another and to connect in an online or traditional social network.

4. Temporal $\mathbb{H}^2$ model discussion

Outside of the quasistatic regime, snapshots $G^{(t)}$ do not fully resemble the static $\mathbb{H}^2$ model—the equilibrium property is in general violated (despite the fact that *each link* was formed via the static-model connection probability corresponding to the pairwise distance at the time of that link's formation). This phenomenon results in reduced clustering because links become spread out across the space rather than being localized amongst neighboring groups of nodes. Degree heterogeneity is also suppressed, as is the case for the temporal HSCM (see Sec. V C), because nodes accumulating large numbers of links due to being near the disk's center do not stay near the disk's center indefinitely. Clustering and heterogeneity arise in the *static* $\mathbb{H}^2$ model due to the correlations in links from the underlying geometry. But in the static model, all links (and nonlinks) arise from the *same* underlying coordinate configuration. When coordinates are dynamical, these correlations are weaker; nodes are linked with probabilities arising as a mixture of past and present coordinate configurations.

VI. LINK UPDATING IN RESPONSE TO HIDDEN-VARIABLE DYNAMICS

Finally, we describe an additional dynamical mechanism that can be incorporated to achieve the equilibrium property *exactly* in TVHMs, while retaining the persistence property, for all values of σ and ω: links are updated *directly in response* to changes in HVs rather than only through link resampling, to keep connection probabilities up to date (we refer to this mechanism as link response). In this model variant, $G^{(t+1)}$'s probability distribution depends on each of $G^{(t)}$, $H^{(t+1)}$, and $H^{(t)}$, rather than on just the former two. We illustrate the mechanism at first in the case of $\omega = 0$. Suppose node pair ij has a link with probability $p_{ij} = f(h_i, h_j)$, and that HVs (h_i, h_j) are updated to become (h'_i, h'_j) in the next time step. To ensure that the pair is then connected with probability $p'_{ij} = f(h'_i, h'_j)$, we selectively delete now-less-likely edges between connected pairs and selectively add now-more-likely edges between unconnected pairs. In particular:

(a) If $p'_{ij} \geqslant p_{ij}$, then $A_{ij} = 1 \Rightarrow A'_{ij} = 1$, and $A_{ij} = 0 \Rightarrow$ add link with probability q^+_{ij},

(b) If $p'_{ij} \leqslant p_{ij}$, then $A_{ij} = 0 \Rightarrow A'_{ij} = 0$, and $A_{ij} = 1 \Rightarrow$ remove link with probability q^-_{ij}.

The outcome needs to result in $\mathbb{P}(A'_{ij} = 1 | h'_i, h'_j) = p'_{ij}$. Thus,

(a) If $p'_{ij} \geqslant p_{ij}$, the new connection probability satisfies $p'_{ij} = p_{ij} + (1 - p_{ij})q^+_{ij}$. Hence, $q^+_{ij} = 1 - \frac{1-p'_{ij}}{1-p_{ij}}$.

(b) If $p'_{ij} \leqslant p_{ij}$, the new connection probability satisfies $1 - p'_{ij} = p_{ij}q^-_{ij} + (1 - p_{ij})$. Hence, $q^-_{ij} = 1 - \frac{p'_{ij}}{p_{ij}}$.

Note that if $p'_{ij} = p_{ij}$, then $q^+_{ij} = q^-_{ij} = 0$; no links will form or break unless pairwise affinities change. Denoting $p^{(t)}_{ij} = f(h^{(t)}_i, h^{(t)}_j)$ for $t \in \{1, ..., T\}$, the graph transition probability given $\mathbf{H}$ becomes

$$\mathcal{P}_G(G^{(t+1)}|G^{(t)}, \mathbf{H}) = \prod_{1 \leqslant i < j \leqslant n} Y_{ij}\left(A^{(t+1)}_{ij}\big|A^{(t)}_{ij}, \mathbf{H}\right), \quad (35)$$

with $Y_{ij} : \{0, 1\} \rightarrow [0, 1]$ denoting the conditional adjacency-element probability distribution. For any $\omega \in [0, 1]$, we have

$$Y_{ij}\left(1\big|A^{(t)}_{ij}, \mathbf{H}\right) = \omega p^{(t+1)}_{ij} + (1 - \omega)K_{ij}\left(A^{(t)}_{ij}, \mathbf{H}\right), \quad (36)$$

where $K_{ij}(A^{(t)}_{ij}, \mathbf{H})$ incorporates the link-response dynamics:

$$K_{ij}\left(A^{(t)}_{ij}, \mathbf{H}\right) = \mathbf{1}\big\{p^{(t+1)}_{ij} \geqslant p^{(t)}_{ij}\big\}\left(q^+_{ij}\left(1 - A^{(t)}_{ij}\right) + A^{(t)}_{ij}\right)$$
$$+ \mathbf{1}\big\{p^{(t+1)}_{ij} \leqslant p^{(t)}_{ij}\big\}(1 - q^-_{ij})A^{(t)}_{ij}. \quad (37)$$

With the inclusion of link response, arbitrary static HV networks can be extended to temporal settings while satisfying the equilibrium property exactly (see Appendix VI for a full derivation) and the persistence property in a tunable fashion. Allowing $\omega > 0$ does not alter the equilibrium property's exact validity and it provides a more tunable level of structural persistence.

With $G^{(t)}$ indistinguishable from a static-model realization, all nonequilibrium phenomena of the types discussed in Secs. V A–V D are prevented—this can either enhance or hinder qualitative realism, depending on the context. If a single node's HV is changed, it will need to reevaluate connections to *all* other nodes for which affinities have changed. This could be realistic in some cases, since nodes themselves may be at the most liberty to reevaluate their connections. In other cases, more gradual structural transitions may be preferred. This model variant could thus serve well as a temporal null model, especially for temporal networks with snapshots well described by an SHVM. Despite *structure* of THVMs with link-response being identical to that of SHVMs, all *dynamical* features are open for study and for comparison to real-world networks.

VII. RELATED WORK

We briefly review existing lines of research related to our study.

Several temporal network models are worth mentioning. Temporal analogs of specific static models have been considered [67–73,122,123], many of which preserve the equilibrium property. Most such models have nondynamic node properties, yielding models related to edge-Markovian networks [99,100,124–126] and dynamic percolation [94–96]. The dynamic-$\mathbb{S}^1$ model [87] is a temporal extension of the static $\mathbb{S}^1$ model [15] consisting of a sequence of independent samples with HVs partially inferred from real data and partially synthetically generated; the dynamics therein resembles

THVMs with $\omega = 1$ and $\sigma = 0$ but with varying average degree parameter across snapshots. Although it is common practice to extend static-model concepts to temporal settings [48–66], many models of temporal networks are instead derived from first principles [127–132] and focus primarily on inference techniques, real-world applicability [133–136], and/or the effects of temporality on spreading [86,99].

Most relevant to THVMs are several existing works with dynamic HVs that influence link dynamics. Several dynamic latent space models [74–77] exist, as do dynamic RGGs [78] (the latter being continuous time and infinite space, with nodes sprinkled as a Poisson process [137–139] and undergoing Brownian motion [140], with links remaining up to date as for THVMs with $\omega = 1$). A model with both dynamic HVs and persistent links [141] was recently introduced, alongside rigorous inference techniques and applications—but not in reference to static network models. Other studies investigated spreading on dynamic RGG-like graphs [79,109]. A few versions of dynamic SBMs are of particular relevance; in one such paper [72], the model is a case of the temporal hyper-SBM studied in Sec. V A with complete edge resampling ($\omega = 1$). Another study was of a temporal hyper-SBM with $\omega < 1$ which thus exhibits both link persistence and group-assignment persistence [73], influencing performance of community detection algorithms and motivating the development of new ones. Another area of relevant work is the rapidly emerging area of *dynamic graph embeddings* [75,142–154], related to the task of *inference of HV trajectories* [155].

We also note some additional works that are less directly related to ours. Adaptive network models (for instance, SIS dynamics [156] alongside contact switching [23,24]), have dynamic node properties that evolve with time and guide network evolution, a commonality with THVMs. Networks with node addition and node removal [157–160] have dynamic node properties (degree values as opposed to HVs) that influence link formation. In the fitness model of growing networks [12], static HVs and dynamic degrees both govern connection probabilities. Some static network models admit dual growing formulations [161]—analogously, if the equilibrium property holds, THVM snapshots can be seen as dynamically produced static-model samples. Indeed, network-rewiring and MCMC algorithms are widely used to sample static networks [162–166]; in stationarity, these can be viewed as temporal networks satisfying the equilibrium property, with a level of persistence tunable via the number of iterations between adjacent snapshots. Dynamic variants of the configuration model [167–169] exemplify this.

VIII. DISCUSSION

In this paper, we have studied temporal network models that are natural counterparts of SHVMs, obtained by inclusion of a dynamic mechanism for node characteristics (jump dynamics or walk dynamics) and dynamic mechanism for link structure (link resampling). Due to the wide generality of the static HV framework, many popular static network models can be made temporal as THVMs.

With a single source of randomness in the static model, which includes $\omega = 1$ with deterministic connectivity (Sec. IV B) and $\sigma = 0$ with fixed initial HVs (Sec. IV C), the

equilibrium property is exactly satisfied and the persistence property is controllable. If, however, the static model has two layers of randomness and links are not completely refreshed each time step ($\sigma > 0$ and $\omega < 1$), THVM snapshots are *not* in general distributed according to the static model. Rather, numerous structural deviations arise, due to links falling out of equilibrium with respect to HVs—for instance, the effective connection probability $\bar{f}(h, h')$ can substantially differ from the affinity function $f(h, h')$ (see Figs. 4 and 7). Despite violating the equilibrium property, such models arise naturally and exhibit qualitative realism in interesting ways—for instance, the appearance of long-ranged links in temporal RGGs (Sec. V A 3) and intergroup links in temporal hyper-SBMs (Sec. V A 3). An exception to the nonequilibrium dynamics arises in the quasistatic regime (Sec. IV A) in which case the equilibrium property is *approximately* satisfied, due to all $A_{ij}^{(t)}$ values arising from an HV configuration closely resembling $H^{(t)}$. A second exception arises if we add a third dynamical mechanism (Sec. VI), namely, link updating in *direct* response to HV changes, which allows *exact* satisfaction of the equilibrium property (see Appendix G) for all (σ, ω). Both situations also lend themselves to tunable satisfaction of the persistence property, governed σ and ω.

An assortment of possible modifications, improvements, and extensions are worth mentioning. Although many questions are open within the present framework, altered dynamics could also be considered. For HV dynamics, correlated motion akin to Langevin dynamics [170,171] could provide insight into the formation and persistence of communities. Altered link structure and link dynamics could be considered as well: some examples include directed and/or weighted links, node-centric link-resampling dynamics [172], or pairwise-individualized resampling rates. Continuous-time formulations of THVMs could allow some theoretical simplifications; continuous time is used in studies of dynamical percolation [94,173,174] and edge-Markovian networks [97–101], which could each be extended to a THVM-like framework by introducing HVs. Our results can also inform future studies of adaptive networks [175–179]; THVMs provide a simple setting in which dynamic node properties influence network evolution. Understanding such settings will provide a baseline for what to expect when coevolutionary feedback is also present. An example of real-world links influencing node properties is social influence, whereby acquainted pairs can become more similar over time [180,181]—or geographically move to closer-by coordinate locations. The inclusion of interdependencies relating to dynamical processes [182,183] can allow for more interesting dynamics and realism but at the cost of increased model complexity.

Real-world networks have dynamic node properties that influence dynamics of link structure. Examples of such phenomena were set forth in Sec. I, ranging across a wide variety of systems and scales. One direct real-world application of THVMs could be to serve as null models [65,184] for evolving networks with dynamic node-properties [75]. Dynamic embedding methods [142–154] or generalizations of inference methods from dynamic SBMs [73] could potentially allow retrieval of **H** (and perhaps also σ, ω, and f) from an observed **G**. Links of real evolving networks may not in general be fully equilibrated relative to the current set of node characteristics,

which is a dynamical behavior exhibited by THVMs *outside of the quasistatic regime*. Hence, in some cases, the equilibrium property and qualitative realism may be *in conflict*, implying that caution should be used when applying static models to snapshots of evolving networks. That said, static models do in many cases accurately describe such snapshots; the internet, for example, has exhibited a clear power-law degree tail for decades [155,185], evidently remaining in equilibrium from the perspective of THVMs (see the discussion in Sec. V C). We expect that the present study will usefully inform general classifications of real-world networks according to the dynamics of node properties and of how those properties influence link dynamics.

APPENDIX A: EFFECTIVE CONNECTION PROBABILITIES

Here we calculate effective connection probabilities for general THVMs with HVs evolving by jump dynamics (HV resampling with probability σ). We define the effective connection probability $\bar{f}(h, h')$ to be the probability of $A_{ij}^{(t)} = 1$ given $h_i^{(t)} = h$ and $h_j^{(t)} = h'$, in the limit as $t \to \infty$. That is,

$$\bar{f}(h, h') = \lim_{t \to \infty} \mathbb{P}\left(A_{ij}^{(t)} = 1 \big| h_i^{(t)} = h, h_j^{(t)} = h'\right), \quad \text{(A1)}$$

where the limit $t \to \infty$ is to wash out any initial condition. Due to the edge-resampling dynamics, the current value of $A_{ij}^{(t)}$ arose from being last resampled at some time $t - s$, with s being a random nonnegative integer having distribution $p_s = \omega(1 - \omega)^s$ (where ω is the probability of link resampling at any given time step). The effective connection probability is given by

$$\bar{f}(h, h') = \sum_{s \geqslant 0} p_s \mathbb{E}\left[f\left(h_i^{(t-s)}, h_j^{(t-s)}\right) \big| h_i^{(t)} = h, h_j^{(t)} = h'\right]. \quad \text{(A2)}$$

To evaluate the above, we introduce a density $P_s(x|h)$, namely, the density of $h_i^{(t-s)}$ (evaluated at x) given $h_i^{(t)} = h$. In our case, by jump dynamics and conditioning on $h_i^{(t)} = h$, we have

$$P_s(x|h) = (1 - \sigma)^s \mathbf{1}_h(x) + (1 - (1 - \sigma)^s)\nu(x) \quad \text{(A3)}$$

because h will have arisen from x after s time steps via either (a) zero jumps having occurred, that event having probability $(1 - \sigma)^s$, or via (b) *at least one* jump having occurred, in which case the density is completely randomized to $\nu(x)$. The expectation value appearing in Eq. (A2) is equal to

$$\mathbb{E}\left[f\left(h_i^{(t-s)}, h_j^{(t-s)}\right) \big| h_i^{(t)} = h, h_j^{(t)} = h'\right]$$

$$= \int_{\mathcal{X}} \int_{\mathcal{X}} f(x, x') P_s(x|h) P_s(x'|h') dx dx', \quad \text{(A4)}$$

which, using Eq. (A3) and integrating over (x, x'), evaluates to

$$(1 - \sigma)^{2s} f(h, h')$$
$$+ (1 - \sigma)^s (1 - (1 - \sigma)^s)(\langle f(\cdot, h') \rangle + \langle f(h, \cdot) \rangle)$$
$$+ (1 - (1 - \sigma)^s)^2 \langle f \rangle, \quad \text{(A5)}$$

where $\langle f(\cdot, h) \rangle = \langle f(h, \cdot) \rangle = \int_{\mathcal{X}} f(h, x) v(x) dx$ and $\langle f \rangle = \int_{\mathcal{X}^2} f(x, x') v(x) v(x') dx dx'$. Finally, plugging Eq. (A5) back into Eq. (A2), using $p_s = \omega(1 - \omega)^s$ and summing the geometric series that appear $[\sum_{s \geqslant 0} y^s = 1/(1 - y)]$, we obtain

$$\bar{f}(h, h') = \alpha_2 f(h, h')$$
$$+ (\alpha_1 - \alpha_2)(\langle f(\cdot, h') \rangle + \langle f(h, \cdot) \rangle)$$
$$+ (1 - 2\alpha_1 + \alpha_2)\langle f \rangle, \quad \text{(A6)}$$

where $\alpha_b = \alpha_b(\sigma, \omega)$ for $b \in \{1, 2\}$ are given by

$$\alpha_b(\sigma, \omega) = \frac{\omega}{1 - (1 - \omega)(1 - \sigma)^b}. \quad \text{(A7)}$$

As an aside, we note that the average degree of the network is independent of (σ, ω). This can be seen by averaging Eq. (A2) over h and h' and making use of $\int_{\mathcal{X}} P_s(x|h) v(h) dh = v(x)$ (which is true because $P_s(x|h)$ describes the stationary distribution, regardless of whether we consider walk dynamics or jump dynamics). The result is $\langle f \rangle$, regardless of σ and ω. This can be seen more directly in the case of jump dynamics by averaging Eq. (A6) over h and h'.

APPENDIX B: TEMPORAL RGG EFFECTIVE CONNECTION PROBABILITY

This section contains calculations of the effective connection probability for RGGs on the unit interval with periodic boundaries and jump dynamics. This result could be obtained from Eq. (A6) but we show here an alternate derivation. The effective connection probability as a function of distances is defined as the probability of two nodes *being connected* given that they are a distance $\mathrm{d}_{ij}^{(t)} = x$ apart, as $t \to \infty$:

$$\bar{f}(x) = \lim_{t \to \infty} \mathbb{P}(A_{ij}^{(t)} = 1 | \mathrm{d}_{ij}^{(t)} = x). \quad \text{(B1)}$$

To calculate the above, we introduce the probability density on distances between node pairs s time steps prior to when the distance value is x, denoted $P_s(y|x)$. We make use of the fact that $\mathrm{d}_{ij}^{(t)}$ can evolve in either of two ways: with probability $(1 - \sigma)^2$ each time step, *neither i nor j jumps*, and thus the density is preserved. Otherwise, one or both do jump and their distance becomes completely randomized. The stationary density of distance x is the uniform on $[0, 1/2]$, i.e., equal to 2 for all $x \in [0, 1/2]$. In a single time advancement, jump dynamics thus yields

$$P_1(y|x) = (1 - \sigma)^2 \mathbf{1}_x(y) + 2(1 - (1 - \sigma)^2). \quad \text{(B2)}$$

Iterating the above logic, $P_s(y|x)$ has two contributions: Either neither node jumps at any time or at least one node jumps at least once. Therefore,

$$P_s(y|x) = (1 - \sigma)^{2s} \mathbf{1}_x(y) + 2(1 - (1 - \sigma)^{2s}). \quad \text{(B3)}$$

We can compute $\bar{f}(x)$ via averaging the affinity $f(h_i, h_j) = \mathbf{1}\{\mathrm{d}_{ij}^{(t)} \leqslant r\}$ over the distance variable. That is,

$$\bar{f}(x) = \sum_{s \geqslant 0} p_s \mathbb{E}[\mathbf{1}\{\mathrm{d}_{ij}^{(t-s)} \leqslant r\} | \mathrm{d}_{ij}^{(t)} = x], \quad \text{(B4)}$$

where the expectation term is

$$\mathbb{E}[\mathbf{1}\{\mathrm{d}_{ij}^{(t-s)} \leqslant r\} | \mathrm{d}_{ij}^{(t)} = x]$$
$$= \int_0^{1/2} P_s(y|x) \mathbf{1}\{y \leqslant r\} dy$$
$$= \int_0^r ((1 - \sigma)^{2s} \mathbf{1}_x(y) + 2(1 - (1 - \sigma)^{2s})) dy$$
$$= (1 - \sigma)^{2s} \mathbf{1}\{x \leqslant r\} + 2r(1 - (1 - \sigma)^{2s}). \quad \text{(B5)}$$

Let $s \in \{0, 1, ...\}$ be the delay since any given edge-indicator was last resampled. Recall that s has distribution $p_s = \omega(1 - \omega)^s$. Then, using the above, we find

$$\bar{f}(x) = \omega \sum_{s \geqslant 0} (1 - \omega)^s (1 - \sigma)^{2s} \mathbf{1}\{x \leqslant r\}$$
$$+ \omega \sum_{s \geqslant 0} (1 - \omega)^s 2r(1 - (1 - \sigma)^{2s})$$
$$= \alpha_2 \mathbf{1}\{x \leqslant r\} + (1 - \alpha_2) 2r, \quad \text{(B6)}$$

with $\alpha_2 = \alpha_2(\sigma, \omega)$ arising from having evaluated sums of geometric series of the form $\sum_{s \geqslant 0} ((1 - \omega)(1 - \sigma)^2)^s$:

$$\alpha_2(\sigma, \omega) = \frac{\omega}{1 - (1 - \omega)(1 - \sigma)^2}. \quad \text{(B7)}$$

APPENDIX C: EFFECTIVE CONNECTION PROBABILITY IN TERMS OF PRODUCTS OF HIDDEN VARIABLES

This section describes effective connection probabilities arising in temporal HSCMs, as studied in Sec. V C. The static-model affinity f is a function of the *product* of HVs, motivating study of the effective connection probability $\bar{f}$ as a function of the product of HVs as well.

Consider one-dimensional HVs $\{h_j\}_{j \in [n]}$ each distributed uniformly on $\mathcal{X} = [0, 1]$. This is applicable to HSCMs via the CDF transform of arbitrary 1D probability densities: If h has density v, then $u = F(h) = \int_{h_-}^h v(h') dh'$ is distributed uniformly on $[0, 1]$ (h_- is the minimum value of h). Denote $P_s(\phi|\psi)$ as the probability density of $\phi = h_i^{(t-s)} h_j^{(t-s)}$ for some arbitrary pair ij given that $h_i^{(t)} h_j^{(t)} = \psi$. Then,

$$\bar{f}(\psi) = \omega \sum_{s \geqslant 0} (1 - \omega)^s \int_0^1 P_s(\phi|\psi) f(\phi) d\phi. \quad \text{(C1)}$$

For products of HVs each independently undergoing jump dynamics, we have

$$P_s(\phi|\psi) = (1 - \sigma)^{2s} \mathbf{1}_\psi(\phi)$$
$$+ (1 - (1 - \sigma)^s)(1 - \sigma)^s p_1(\phi|\psi)$$
$$+ (1 - (1 - \sigma)^s)^2 \mu(\phi), \quad \text{(C2)}$$

with $\mu(\phi)$ denoting the product density of HVs and $p_1(\phi|\psi)$ the product HV density conditioned on a single jump. Then,

$$\bar{f}(\psi) = \alpha f(\psi) + \omega \sum_{s \geqslant 0} ((1-\sigma)(1-\omega))^s (1 - (1-\sigma)^s)$$

$$\times \int_0^1 f(\phi) p_1(\phi|\psi) d\phi$$

$$+ \omega \sum_{s \geqslant 0} (1-\omega)^s (1-(1-\sigma)^s)^2 \int_0^1 f(\phi)\mu(\phi)d\phi.$$

$$\text{(C3)}$$

Note that $\int_0^1 f(\phi)\mu(\phi)d\phi = \langle f \rangle = \langle k \rangle/n$. Then, evaluating sums,

$$\bar{f}(\psi) = \alpha_2 f(\psi) + (\alpha_1 - \alpha_2)f_1(\psi) + (1 - 2\alpha_1 + \alpha_2)\langle f \rangle,$$

$$\text{(C4)}$$

with $\alpha_b = \omega/(1 - (1-\omega)(1-\sigma)^b)$, and the quantity $f_1(\psi)$ being defined as

$$f_1(\psi) = \int f(\phi) p_1(\phi|\psi)d\phi, \qquad \text{(C5)}$$

where $p_1(\phi|\psi)$ is the distribution of the product of a uniform random variable and of one factor of a product, given that the value of that product is ψ. In the following, we walk through the remaining required calculations to obtain $f_1(\psi)$.

1. Finding $p(x|xy = \psi)$

Suppose that x and y are sampled uniformly on [0,1]. Now condition on the fact that their product, xy, takes on the particular value $xy = \psi$. Then, what is the probability density of x alone? Note first that it must reside in $[\psi, 1]$, since ψ is the product of two numbers each in the range [0,1], i.e., each reducing the value of the product. Within the acceptable range, the density is obtained as follows:

$$p(x|xy = \psi) \propto \int_0^1 \mathbf{1}_\psi(xy)dy$$

$$\propto \frac{1}{x} \int_0^1 \mathbf{1}_{\psi/x}(y)dy$$

$$= 1/x, \qquad \text{(C6)}$$

where the ratio ψ/x is guaranteed to be in the range [0,1] since $x \geqslant \psi$. Combining the above with the range of acceptable values of x given $xy = \psi$, we have proportionality

$$p(x|xy = \psi) = c\frac{\mathbf{1}\{x \in [\psi, 1]\}}{x}, \qquad \text{(C7)}$$

and c is determined by normalization:

$$1 = \int_0^1 p(x|xy=\psi)dx = c\int_\psi^1 \frac{dx}{x} = c\ln(1/\psi)$$

$$\Rightarrow c = \frac{1}{\ln(1/\psi)}. \qquad \text{(C8)}$$

Therefore,

$$p(x|xy = \psi) = \frac{\mathbf{1}\{x \in [\psi, 1]\}}{x\ln(1/\psi)}, \qquad \text{(C9)}$$

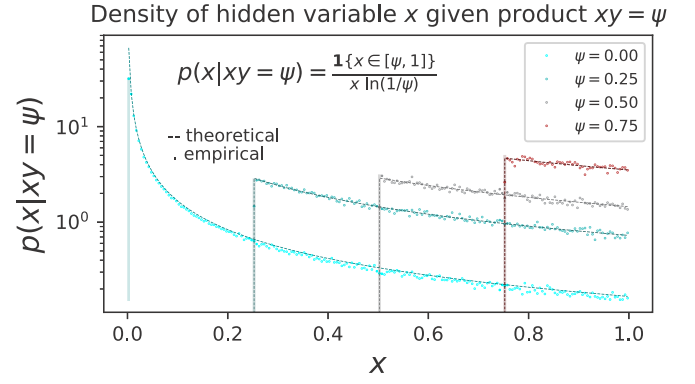as is confirmed numerically in Fig. 8.

FIG. 8. The probability density of the value of one member x of a product xy conditioned on $xy = \psi$. In the absence of the conditionality, both x and y are distributed uniformly on [0,1].

2. Finding $p_1(\phi|\psi)$

Now suppose that one variable, say y, undergoes a random jump (i.e., is resampled) and thus becomes a new uniform variable on [0,1]. The equality $xy = \psi$ no longer holds, but since it did hold prior to the jump, the variable x remains distributed according to $p(x|xy = \psi)$. Therefore the *new* product's value, which we denote by $\phi = xy'$ (where y' is the postjump version of y), has a density $p_1(\phi|\psi)$ of the following form:

$$p_1(\phi|\psi) = \int_0^1 \mathbf{1}\{y' \in [0, 1]\} p\left(\frac{\phi}{y'}\bigg|xy = \psi\right)\frac{1}{y'}dy'$$

$$= \int_0^1 \frac{\mathbf{1}\{\phi/y' \in [\psi, 1]\}}{(\phi/y')\ln(1/\psi)}\frac{dy'}{y'}$$

$$= \frac{1}{\phi\ln(1/\psi)}\int_0^1 \mathbf{1}\{\phi/y' \in [\psi, 1]\}dy'. \quad \text{(C10)}$$

Continuing with a change of variables,

$$p_1(\phi|\psi) = \frac{1}{\ln(1/\psi)}\int_0^{1/\phi} \mathbf{1}\{y'/\phi \in [1, 1/\psi]\}d(y'/\phi)$$

$$= \frac{\min(1/\phi, 1/\psi) - 1}{\ln(1/\psi)}. \qquad \text{(C11)}$$

The above is validated numerically in Fig. 9.

3. Calculating $\bar{f}_1(\psi)$

We now average the affinity over $p_1(\phi|\psi)$, to get the contribution to the effective connection probability coming from *one* HV jumping. This goes as

$$\bar{f}_1(\psi) = \int_0^1 f(\phi)p_1(\phi|\psi)d\phi$$

$$= \int_0^1 f(\phi)\frac{\min(1/\phi, 1/\psi) - 1}{\ln(1/\psi)}d\phi$$

$$= \frac{1}{\ln(1/\psi)}\left(\frac{1}{\psi}\int_0^\psi f(\phi)d\phi + \int_\psi^1 \frac{f(\phi)}{\phi}d\phi - 1\right).$$
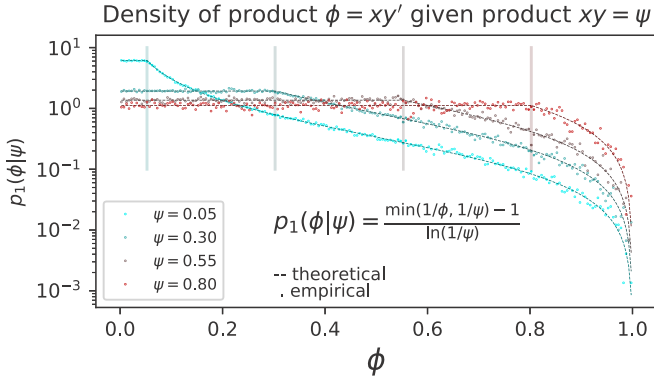
$$\text{(C12)}$$

FIG. 9. The probability density of the value ϕ of the product $\phi = xy'$, where y' is uniformly sampled after having previously had random value y and where xy was conditioned to have value $xy = \psi$. Without any conditioning, all three x, y, y' have marginal density uniform on [0,1].

Using Eq. (C12), we can compute $\bar{f}(\psi)$ for a given $f(\psi)$ via Eq. (C4).

APPENDIX D: WALK DYNAMICS

Here we describe walk dynamics in detail. Throughout this paper, walk dynamics in one dimension is simulated by first mapping random variables to the unit interval (by the inverse-CDF method [186]), doing a random walk on [0,1], then mapping back. For any one-dimensional probability density $\nu(x)$ where $x \in \mathbb{R}_+$, we define random variable $u(x) = F_\nu(x)$, where $F_\nu(x) = \int_0^x \nu(y)dy$. The probability density of $u(x)$ is the uniform on [0,1]. A random walk on [0,1] is constructed via addition of uniform noise in the range $[-2\sigma, 2\sigma]$, parameterized by $\sigma \in [0, 1]$. That is, after rescaling we have HV dynamics:

$$\mathcal{P}_h(u'|u) = \frac{\mathbf{1}\{|u' - u| \leqslant 2\sigma\}}{4\sigma}. \tag{D1}$$

Note that the choice of $[-2\sigma, 2\sigma]$ results in a mean jump length equal to σ, neglecting boundary conditions; when implementing boundary conditions, one needs only to adjust the probability density $\mathcal{P}_h(u'|u)$ according to the circumstance. See Appendix E for the case of reflecting boundaries.

Drawing $h^{(1)}$ from ν, we initialize $u^{(1)} = F_\nu(h^{(1)})$ and iteratively time advance as per the above to obtain $\{u^{(t)}\}_{t=1}^T$. We then simply transform back via $h^{(t)} = F_\nu^{-1}(u^{(t)})$ to obtain one-dimensional dynamics whose stationary distribution is ν.

In dimensions greater than one, walk dynamics can be simulated by first taking the multidimensional inverse-CDF transform, mapping the space $\mathcal{X}$ to a unit cube. Walk dynamics can then be performed with whatever custom boundary conditions are required on that unit cube (boundary conditions that correspond to those of $\mathcal{X}$) and the results can then be mapped back to the original space $\mathcal{X}$. For example, in the $\mathbb{H}^2$ model (Appendix F), increments of change in the angular and radial coordinates were chosen to be independent; this option was taken for simplicity but nonindependent cases would also be interesting to explore. Any transitional probability density

preserving the uniform on the unit cube would fall within the same framework.

APPENDIX E: WALK DYNAMICS WITH REFLECTING BOUNDARY CONDITIONS

In this Appendix we study walk dynamics on $\mathcal{X} = [0, 1]$ with *reflecting* boundary conditions under uniform noise. In particular, we show that the stationary density is uniform on [0,1]. In turn, that implies that arbitrary 1D dynamics with density $\nu(h)$ can be made into a random walk of this type, by mapping initial h values to [0,1] via the inverse-CDF transform, performing the reflecting random walk on [0,1], then transforming the random walk trajectories back to the original space (see Appendix D).

Let $\mathcal{X} = [0, 1]$ be the HV space and denote by $x \leftarrow U[0, 1]$ the value of a HV. Then let $\hat{x} \in [-r, 1 + r]$ be an intermediate variable defined as $\hat{x} = x + u$, where $u \leftarrow U[-r, r]$ is the uniform additive noise which we use to simulate walk-dynamics. Lastly, let $x' = Z(\hat{x})$ be the reflected variable, where the function Z encodes the reflecting boundary conditions. Note that values of x' in the ranges $[0, r]$ and $[1 - r, 1]$ are obtained from one of two different of values of $\hat{x}$: the case when reflected and the case when not reflected. To transform the density of $\hat{x}$ into that of x', we write x' as a function of $\hat{z}$, as $x' = Z(\hat{x})$ and use the generalized change-of-variables formula for probability densities [187]. We denote the densities of $x, \hat{x}, x'$ as $P(x)$, $\hat{P}(\hat{x})$, and $P'(x')$, respectively. The density of $\hat{x}$ given x is

$$\hat{P}(\hat{x}|x) = \frac{\mathbf{1}\{\hat{x} \in [x - r, x + r]\}}{2r} = \frac{\mathbf{1}\{x \in [\hat{x} - r, \hat{x} + r]\}}{2r}. \tag{E1}$$

Since x is uniform on [0,1] the density of $\hat{x}$ is then

$$\begin{aligned}
\hat{P}(\hat{x}) &= \int_0^1 \hat{P}(\hat{x}|x)dx \\
&= \frac{1}{2r} \int_0^1 \mathbf{1}\{x \in [\hat{x} - r, \hat{x} + r]\}dx \\
&= \frac{1}{2r}|[0, 1] \cup [\hat{x} - r, \hat{x} + r]| \tag{E2}
\end{aligned}$$

or

$$\hat{P}(\hat{x}) = \frac{1}{2r}
\begin{cases}
\hat{x} + r, & \hat{x} < r \\
2r & \hat{x} \in [r, 1 - r] \\
1 + r - \hat{x}, & \hat{x} > 1 - r,
\end{cases} \tag{E3}$$

where the $\hat{x}$-dependent coefficients of the first and third terms arise from reflections of the form $\hat{x} - (-r)$ and $1 - (\hat{x} - 1)$. We seek a function $Z : [-r, 1 + r] \to [0, 1]$ that encodes the reflection properties of the walk dynamics. The necessary Z is given by

$$Z(\hat{x}) =
\begin{cases}
-\hat{x}, & \hat{x} < 0 \\
\hat{x}, & \hat{x} \in [0, 1] \\
2 - \hat{x}, & \hat{x} > 1.
\end{cases} \tag{E4}$$

The values of $\hat{x}$ mapping to a given value of x', namely, those making up the inverse of Z, are given by

$$\{\hat{x} : Z(\hat{x}) = x'\} = \begin{cases} \{-x', x'\}, & x' < r \\ \{x'\}, & x' \in [r, 1-r] \\ \{x', 2-x'\}, & x' > 1-r. \end{cases} \quad (E5)$$

Let us compute the derivative of $Z(\hat{x})$, neglecting the measure-zero points of 0 and 1:

$$\frac{dZ(\hat{x})}{d\hat{x}} = \begin{cases} -1, & \hat{x} < 0 \\ 1, & \hat{x} \in (0, 1) \\ -1, & \hat{x} > 1. \end{cases} \quad (E6)$$

We now transform to find the density after one step of dynamics, as

$$\begin{aligned} P'(x') &= \sum_{\hat{x}:Z(\hat{x})=x'} \left| \frac{dZ(\hat{x})}{d\hat{x}} \right|^{-1} \hat{P}(\hat{x}) \\ &= \begin{cases} \hat{P}(-x') + \hat{P}(x'), & x' < r \\ \hat{P}(x'), & x' \in [r, 1-r] \\ \hat{P}(x') + \hat{P}(2-x'), & x' > 1-r \end{cases} \\ &= 1. \end{aligned} \quad (E7)$$

Therefore, the stationary distribution is uniform.

APPENDIX F: HYPERBOLIC WALK DYNAMICS

To sample $\tilde{h} = (\tilde{r}, \tilde{\theta})$ and also to sample $h_j^{(1)}$ (a coordinate from the initial time step, i.e., the static $\mathbb{H}^2$ model), we first draw two independent random variables U_r and U_θ, each from the uniform distribution on [0,1]. These are then set equal to the cumulative density functions of $\nu_{\rm rad}$ and $\nu_{\rm ang}$, evaluated at $\tilde{r}$ and $\tilde{\theta}$, respectively:

$$U_\theta = \int_0^{\tilde{\theta}} \nu_{\rm ang}(\theta) d\theta = \frac{\tilde{\theta}}{2\pi},$$

$$U_r = \int_0^{\tilde{r}} \nu_{\rm rad}(r) dr = \frac{\cosh\left(\frac{\gamma-1}{2}\tilde{r}\right) - 1}{\cosh\left(\frac{\gamma-1}{2}R\right) - 1}. \quad (F1)$$

From the above, we can solve to obtain $\tilde{h}$ in terms of (U_r, U_θ):

$$\tilde{\theta} = 2\pi U_\theta,$$

$$\tilde{r} = \frac{2}{\gamma-1} \cosh^{-1}\left(1 + \left(\cosh\left(\frac{\gamma-1}{2}R\right) - 1\right) U_r\right). \quad (F2)$$

In the temporal setting, those initial variables are set to $U_\theta^{(1)}$ and $U_r^{(1)}$, after which we perform walk dynamics on the transformed variables to obtain $(U_\theta^{(t)}, U_r^{(t)})$ for $t \in \{2, ..., T\}$. Walk dynamics occurs independently for the two variables, with periodic boundary conditions for angular coordinates and reflecting boundary conditions for radial coordinates.

Note that we use reflecting boundary conditions for the radial coordinate, rather than, for example, periodic boundary conditions or reflecting boundary conditions with an associated angular reversal at any time step that a node reflects from the origin of the radial coordinate (as would also seem like a natural choice for the disk). The reason to not incorporate such angular flipping is due to the interpretation of the angular

coordinates as similarity-encoding variables [188]. From that perspective, it is more realistic to have nodes reflect off of the disk's origin and retain their similarity coordinates rather than to pass through the origin and reverse their similarity coordinates.

APPENDIX G: STATIONARITY WITH LINK RESPONSE

In this Appendix, we show that the static-model graph probability distribution is preserved via the effect of link response as described in Sec. VI. Specifically, we show that

$$\int_{\mathcal{H}} \left(\sum_{G \in \mathcal{G}} \mathbb{P}(G|H) P_{H,H'}^{G \to G'} \right) \rho(H) dH = \mathbb{P}(G'|H'), \quad (G1)$$

where $P_{H^{(t)}, H^{(t+1)}}^{G^{(t)} \to G^{(t+1)}} = \mathcal{P}_G(G^{(t+1)}|G^{(t)}, H^{(t+1)}, H^{(t)})$. We for now set $\omega = 0$ and later argue that link resampling does not influence the results in question. First, we note that the transition probability given (H, H') is separable: $P_{H,H'}^{G \to G'} = \prod_{1 \leq i < j \leq n} P_{ij}^{A_{ij} \to A'_{ij}}$, with transition probability $P_{ij}^{\alpha \to \beta} = \mathbb{P}(A'_{ij} = \beta | A_{ij} = \alpha, h'_i, h'_j, h_i, h_j)$. Denoting $f_{ij} = f(h_i, h_j)$ and $f'_{ij} = f(h'_i, h'_j)$, we evaluate the different transition probabilities:

$$P_{ij}^{1 \to 1} = \mathbf{1}\{f'_{ij} \geq f_{ij}\} + (1 - q_{ij}^-)\mathbf{1}\{f'_{ij} < f_{ij}\},$$

$$P_{ij}^{0 \to 0} = \mathbf{1}\{f'_{ij} < f_{ij}\} + (1 - q_{ij}^+)\mathbf{1}\{f'_{ij} \geq f_{ij}\}, \quad (G2)$$

with $q_{ij}^- = 1 - f'_{ij}/f_{ij}$, $q_{ij}^+ = 1 - (1 - f'_{ij})/(1 - f_{ij})$ as defined in Sec. VI. The remaining probabilities are obtained by normalization:

$$P_{ij}^{1 \to 0} = 1 - P_{ij}^{1 \to 1} = q_{ij}^- \mathbf{1}\{f'_{ij} < f_{ij}\},$$

$$P_{ij}^{0 \to 1} = 1 - P_{ij}^{0 \to 0} = q_{ij}^+ \mathbf{1}\{f'_{ij} \geq f_{ij}\}. \quad (G3)$$

Noting that $P_{H,H'}^{G \to G'}$ and $\mathbb{P}(G|H)$ are both separable into a product over $ij : 1 \leq i < j \leq n$, we write

$$\mathbb{P}(G|H) P_{H,H'}^{G \to G'} = \prod_{1 \leq i < j \leq n} f_{ij}^{A_{ij}} (1 - f_{ij})^{1 - A_{ij}} P_{ij}^{A_{ij} \to A'_{ij}}. \quad (G4)$$

The sum over all graphs G of this product becomes a product over all pairs ij of a sum over $A_{ij} \in \{0, 1\}$:

$$\sum_{G \in \mathcal{G}} \prod_{1 \leq i < j \leq n} y(A_{ij}) = \prod_{1 \leq i < j \leq n} \sum_{A_{ij} \in \{0,1\}} y(A_{ij}). \quad (G5)$$

Using the above, and Eq. (5), the parenthesized term in Eq. (G1) is equal to

$$\prod_{ij:A'_{ij}=0} \left(f_{ij} P_{ij}^{1 \to 0} + (1 - f_{ij}) P_{ij}^{0 \to 0}\right)$$

$$\times \prod_{ij:A'_{ij}=1} \left(f_{ij} P_{ij}^{1 \to 1} + (1 - f_{ij}) P_{ij}^{0 \to 1}\right). \quad (G6)$$

Applying Eqs. (G2) and (G3) and using the expressions for $q_{ij}^\pm$, as well as the facts that $\mathbf{1}\{f'_{ij} \geq f_{ij}\} + \mathbf{1}\{f'_{ij} < f_{ij}\} = 1$ and $\int_{\mathcal{H}} \rho(H) dH = 1$, Equation (G1) becomes

$$\prod_{ij:A'_{ij}=1} f'_{ij} \prod_{ij:A'_{ij}=0} (1 - f'_{ij}) = \mathbb{P}(G'|H'). \quad (G7)$$

The left-hand side of the above is exactly the static model's graph probability distribution given a HV configuration [see Eq. (5) of the main text]. Thus the SVHM is the stationary distribution of time advancements with the link-response mechanism.

To show that these results hold even upon inclusion of the link-resampling mechanism (allowing $\omega > 0$), consider the following reasoning. Regardless of what the link-response step yielded, each node-pair undergoing link resampling at rate ω will result in either (a) linking according to the connection probability of the newly updated HV configuration (with probability ω) or (b) linking as before ($\omega = 0$), without altering the connection probability. Given the fact that stationarity holds without link resampling, in the latter case we also have a connection probability equal to that of the updated HV configuration.

Thus, upon inclusion of the link-response mechanism whereby both $H^{(t+1)}$ and $H^{(t)}$ impact the transition from $G^{(t)}$ to $G^{(t+1)}$, we have temporal extensions of arbitrary SHVMs that *exactly* satisfy the equilibrium property, while retaining the persistence property. Such a link-response mechanism may better reflect reality in cases where connectivity among nodes changes directly in response to changes in their internal characteristics.

APPENDIX H: DISCRETE HIDDEN VARIABLES

We consider THVMs formulated with discrete HVs and describe their relation to continous-HV models.

We take, for example, the case of SBMs, described in Sec. V A entirely in terms of discrete HVs, namely, group indices which are naturally thought of as discrete. We then have a set of discrete HVs $\{q_j\}_{j \in [n]}$, each distributed into a discrete set $[m] = \{1, ..., m\}$ according to a probability distribution $\varrho : [m] \to [0, 1]$ and connecting via a discrete affinity function $f_{q,q'}$.

In a dual continuous-HV system which maps to the above-described discrete system, suppose each node j's HV h_j has uniform density on [0,1] and pairwise affinities are encoded in a piecewise constant graphon function according to occupancy of points in nonoverlapping subregions $\{L_w\}_{w \in [m]} \subseteq [0, 1]^m$ such that $|L_w| = \varrho_w$ and such that

$$f(h, h') = \sum_{(w,z) \in [m]^2} f_{w,z} \mathbf{1}\{h \in L_w, h' \in L_z\}. \tag{H1}$$

Discrete node labels can also be written directly in terms of continuous HV values as

$$q_i = \sum_{q \in [m]} q \mathbf{1}\{h_i \in L_q\}. \tag{H2}$$

The probability distribution ϱ thus arises from integration of the uniform density on [0,1], namely, $\nu(h) = 1$, over the regions $\{L_q\}_{q \in [m]}$ corresponding to specific group-labels $q \in [m]$:

$$\varrho_q = \int_{\mathcal{X}} \nu(h) \mathbf{1}\{h \in L_q\} dh = \int_{L_q} dh = |L_q|. \tag{H3}$$

In the temporal setting, we can again relate discrete HVs to continuous ones. To reproduce the HV-resampling dynamics for temporal SBMs, we can simply have continuous HVs undergo jump dynamics in [0,1]. Jumping to a random point in [0,1] amounts to jumping into a random subset L_q with probability $\varrho_q = |L_q|$.

[1] H. Janwa, S. Massey, J. Velev, and B. B. Mishra, On the origin of biomolecular networks, Front. Genet. **10**, 240 (2019).

[2] N. Boers, B. Goswami, A. Rheinwalt, B. Bookhagen, B. Hoskins, and J. Kurths, Complex networks reveal global pattern of extreme-rainfall teleconnections, Nature **566**, 373 (2019).

[3] L. F. Costa, O. N Oliveira Jr, G. Travieso, F. A. Rodrigues, P. R. Villas Boas, L. Antiqueira, M. P. Viana, and L. E. Correa Rocha, Analyzing and modeling real-world phenomena with complex networks: A survey of applications, Adv. Phys. **60**, 329 (2011).

[4] L. E. C. Rocha, F. Liljeros, and P. Holme, Information dynamics shape the sexual networks of internet-mediated prostitution, Proc. Natl. Acad. Sci. **107**, 5706 (2010).

[5] G. B. West, J. H. Brown, and B. J. Enquist, A general model for the origin of allometric scaling laws in biology, Science **276**, 122 (1997).

[6] R. Pastor-Satorras and A. Vespignani, *Evolution and Structure of the Internet: A Statistical Physics Approach* (Cambridge University Press, Cambridge, United Kingdom, 2004).

[7] M. Zheng, A. Allard, P. Hagmann, Y. Alemán-Gómez, and M. Á. Serrano, Geometric renormalization unravels self-similarity of the multiscale human connectome, Proc. Natl. Acad. Sci. **117**, 20244 (2020).

[8] G. Cimini, T. Squartini, F. Saracco, D. Garlaschelli, A. Gabrielli, and G. Caldarelli, The statistical physics of real-world networks, Nat. Rev. Phys. **1**, 58 (2019).

[9] H. Kim, H. B. Smith, C. Mathis, J. Raymond, and S. I. Walker, Universal scaling across biochemical networks on earth, Sci. Adv. **5**, eaau0149 (2019).

[10] P. L. Krapivsky and S. Redner, A statistical physics perspective on web growth, Computer Networks **39**, 261 (2002).

[11] A.-L. Barabási and R. Albert, Emergence of scaling in random networks, Science **286**, 509 (1999).

[12] G. Bianconi and A.-L. Barabási, Competition and multiscaling in evolving networks, Europhys. Lett. **54**, 436 (2001).

[13] G. Caldarelli, A. Capocci, P. De Los Rios, and M. A. Muñoz, Scale-free networks from varying vertex intrinsic fitness, Phys. Rev. Lett. **89**, 258702 (2002).

[14] M. Barthelemy, *Morphogenesis of Spatial Networks* (Springer, Berlin, Germany, 2018).

[15] D. Krioukov, F. Papadopoulos, M. Kitsak, A. Vahdat, and M. Boguná, Hyperbolic geometry of complex networks, Phys. Rev. E **82**, 036106 (2010).

[16] M. Á. Serrano, M. Boguná, and F. Sagués, Uncovering the hidden geometry behind metabolic networks, Mol. BioSyst. **8**, 843 (2012).

[17] M. Kitsak, F. Papadopoulos, and D. Krioukov, Latent geometry of bipartite networks, Phys. Rev. E **95**, 032309 (2017).

[18] M. Boguná and R. Pastor-Satorras, Class of correlated random networks with hidden variables, Phys. Rev. E **68**, 036112 (2003).

[19] M. Newman, *Networks* (Oxford University Press, Oxford, United Kingdom, 2018).

[20] B. Karrer and M. E. J. Newman, Stochastic blockmodels and community structure in networks, Phys. Rev. E **83**, 016107 (2011).

[21] M. Penrose, *Random Geometric Graphs*, Vol. 5 (Oxford University Press, Oxford, United Kingdom, 2003).

[22] P. van der Hoorn, G. Lippner, and D. Krioukov, Sparse maximum-entropy random graphs with a given power-law degree distribution, J. Stat. Phys. **173**, 806 (2018).

[23] S. Risau-Gusmán and D. H. Zanette, Contact switching as a control strategy for epidemic outbreaks, J. Theor. Biol. **257**, 52 (2009).

[24] S. Piankoranee and S. Limkumnerd, Effects of global and local rewiring on sis epidemic adaptive networks, in Journal of Physics: Conference Series, Vol. 1144 (IOP Publishing, Bristol, United Kingdom, 2018), p. 012080.

[25] C. Huepe, G. Zschaler, A.-L. Do, and T. Gross, Adaptive-network models of swarm dynamics, New J. Phys. **13**, 073022 (2011).

[26] V. Marceau, P.-A. Noël, L. Hébert-Dufresne, A. Allard, and L. J. Dubé, Adaptive networks: Coevolution of disease and topology, Phys. Rev. E **82**, 036116 (2010).

[27] G. Demirel, F. Vazquez, G. A. Böhme, and T. Gross, Moment-closure approximations for discrete adaptive networks, Physica D **267**, 68 (2014).

[28] T. Gross and H. Sayama, Adaptive networks, *Adaptive Networks* (Springer, Berlin, Germany, 2009), pp. 1–8.

[29] I. B. Crabtree and S. J. Soltysiak, Identifying and tracking changing interests, Int. J. Digital Libraries **2**, 38 (1998).

[30] B. B. Chapman, C. Brönmark, J.-Å. Nilsson, and L.-A. Hansson, The ecology and evolution of partial migration, Oikos **120**, 1764 (2011).

[31] Y. Vardanis, R. H. G. Klaassen, R. Strandberg, and T. Alerstam, Individuality in bird migration: Routes and timing, Biol. Lett. **7**, 502 (2011).

[32] S. Altizer, R. Bartel, and B. A. Han, Animal migration and infectious disease risk, Science **331**, 296 (2011).

[33] M. Pfeffer and G. Dobler, Emergence of zoonotic arboviruses by animal trade and migration, Parasites & Vectors **3**, 35 (2010).

[34] A. M. Hein, C. Hou, and J. F. Gillooly, Energetic and biomechanical constraints on animal migration distance, Ecol. Lett. **15**, 104 (2012).

[35] S. P. Carroll, A. P. Hendry, D. N. Reznick, and C. W. Fox, Evolution on ecological time-scales, Functional Ecol. **21**, 387 (2007).

[36] T. Held, A. Nourmohammad, and M. Lässig, Adaptive evolution of molecular phenotypes, J. Stat. Mech.: Theory Exp. (2014) P09029.

[37] H. W. Volberda and A. Y. Lewin, Co-evolutionary dynamics within and between firms: From evolution to co-evolution, J. Manage. Stud. **40**, 2111 (2003).

[38] M. Stoica and M. Schindehutte, Understanding adaptation in small firms: Links to culture and performance, J. Dev. Entrepreneurship **4**, 1 (1999).

[39] K. M. Johnson, Demographic trends in rural and small town america, Reports on Rural America **1** (2006), doi: 10.34051/p/2020.6.

[40] D. Myers, Demographic dynamism and metropolitan change: Comparing Los Angeles, New York, Chicago, and Washington, DC, Housing Policy Debate **10**, 919 (1999).

[41] J. Raimbault, Modeling the co-evolution of cities and networks, arXiv:1804.09430.

[42] S. Kuhar, L. Feng, S. Vidan, M. Ross, M. Hatten, and N. Heintz, Changing patterns of gene expression define four stages of cerebellar granule neuron differentiation, Development **117**, 97 (1993).

[43] M. A. McCormack, K. M. Rosen, L. Villa-Komaroff, and G. D. Mower, Changes in immediate early gene expression during postnatal development of cat cortex and cerebellum, Mol. Brain Res. **12**, 215 (1992).

[44] M. M. Dalvand, S. B. Z. Azami, and H. Tarimoradi, Long-term load forecasting of Iranian power grid using fuzzy and artificial neural networks, in *2008 43rd International Universities Power Engineering Conference* (IEEE, New York, United States, 2008), pp. 1–4.

[45] M. De Felice, A. Alessandri, and P. M. Ruti, Electricity demand forecasting over italy: Potential benefits using numerical weather prediction models, Electr. Power Syst. Res. **104**, 71 (2013).

[46] N. Pasichnyk, M. Dyvak, and R. Pasichnyk, Mathematical modeling of website quality characteristics in dynamics, in *Journal of Applied Computer Science*, Vol. 22 (Technical University Press, Lodz, Poland, 2014), pp. 171–183.

[47] S. J. Bean, Emerging and continuing trends in vaccine opposition website content, Vaccine **29**, 1874 (2011).

[48] V. Nicosia, J. Tang, C. Mascolo, M. Musolesi, G. Russo, and V. Latora, Graph metrics for temporal networks, in *Temporal Networks* (Springer, Berlin, Germany, 2013), pp. 15–40.

[49] E. Ortiz, M. Starnini, and M. Á. Serrano, Navigability of temporal networks in hyperbolic space, Sci. Rep. **7**, 15054 (2017).

[50] D. Taylor, S. A. Myers, A. Clauset, M. A. Porter, and P. J. Mucha, Eigenvector-based centrality measures for temporal networks, Multiscale Model. Simul. **15**, 537 (2017).

[51] H. Kim and R. Anderson, Temporal node centrality in complex networks, Phys. Rev. E **85**, 026107 (2012).

[52] R. K. Pan and J. Saramäki, Path lengths, correlations, and centrality in temporal networks, Phys. Rev. E **84**, 016105 (2011).

[53] A. Li, S. P. Cornelius, Y.-Y. Liu, L. Wang, and A.-L. Barabási, The fundamental advantages of temporal networks, Science **358**, 1042 (2017).

[54] S. Liu, N. Perra, M. Karsai, and A. Vespignani, Controlling Contagion Processes in Activity Driven Networks, Phys. Rev. Lett. **112**, 118702 (2014).

[55] N. Perra, A. Baronchelli, D. Mocanu, B. Gonçalves, R. Pastor-Satorras, and A. Vespignani, Random Walks and Search in Time-Varying Networks, Phys. Rev. Lett. **109**, 238701 (2012).

[56] A. Paranjape, A. R. Benson, and J. Leskovec, Motifs in temporal networks, in *Proceedings of the Tenth ACM International Conference on Web Search and Data Mining* (ACM, New York, United States, 2017), pp. 601–610.

[57] P. Holme, Temporal network structures controlling disease spreading, Phys. Rev. E **94**, 022305 (2016).

[58] Q.-H. Liu, X. Xiong, Q. Zhang, and N. Perra, Epidemic spreading on time-varying multiplex networks, Phys. Rev. E **98**, 062303 (2018).

[59] M. Nadini, K. Sun, E. Ubaldi, M. Starnini, A. Rizzo, and N. Perra, Epidemic spreading in modular time-varying networks, Sci. Rep. **8**, 2352 (2018).

[60] N. Masuda and P. Holme, *Temporal Network Epidemiology* (Springer, Berlin, Germany, 2017).

[61] K. Sun, A. Baronchelli, and N. Perra, Contrasting effects of strong ties on sir and sis processes in temporal networks, Eur. Phys. J. B **88**, 326 (2015).

[62] D. Li, D. Han, J. Ma, M. Sun, L. Tian, T. Khouw, and H. E. Stanley, Opinion dynamics in activity-driven networks, Europhys. Lett. **120**, 28002 (2018).

[63] D. M. Dunlavy, T. G. Kolda, and E. Acar, Temporal link prediction using matrix and tensor factorizations, ACM Trans. Knowledge Discovery from Data (TKDD) **5**, 10 (2011).

[64] Y. Dhote, N. Mishra, and S. Sharma, Survey and analysis of temporal link prediction in online social networks, in *2013 International Conference on Advances in Computing, Communications and Informatics (ICACCI)* (IEEE, New York, United States, 2013), pp. 1178–1183.

[65] M. Sarzynska, E. A. Leicht, G. Chowell, and M. A. Porter, Null models for community detection in spatially embedded, temporal networks, J. Complex Networks **4**, 363 (2016).

[66] L. Gauvin, A. Panisson, and C. Cattuto, Detecting the community structure and activity patterns of temporal networks: A non-negative tensor factorization approach, PLoS One **9**, e86028 (2014).

[67] T. P. Peixoto and M. Rosvall, Modelling sequences and temporal networks with dynamic community structures, Nat. Commun. **8**, 582 (2017).

[68] K. S. Xu and A. O. Hero, Dynamic stochastic blockmodels for time-evolving social networks, IEEE J. Selected Top. Signal Processing **8**, 552 (2014).

[69] K. Xu, Stochastic block transition models for dynamic networks, in *Artificial Intelligence and Statistics*, edited by G. Lebanon and S. V. N. Vishwanathan, Vol. 38 (Proceedings of Machine Learning Research, San Juan, United States, 2015), pp. 1079–1087.

[70] C. Matias and V. Miele, Statistical clustering of temporal networks through a dynamic stochastic block model, J. Royal Stat. Soc.: Series B (Stat. Methodol.) **79**, 1119 (2017).

[71] M. Pensky and T. Zhang, Spectral clustering in the dynamic stochastic block model, Electron. J. Stat. **13**, 678 (2019).

[72] A. Ghasemian, P. Zhang, A. Clauset, C. Moore, and L. Peel, Detectability Thresholds and Optimal Algorithms for Community Structure in Dynamic Networks, Phys. Rev. X **6**, 031005 (2016).

[73] P. Barucca, F. Lillo, P. Mazzarisi, and D. Tantari, Disentangling group and link persistence in dynamic stochastic block models, J. Stat. Mech.: Theory Exp. (2018) 123407.

[74] D. K. Sewell and Y. Chen, Latent space models for dynamic networks with weighted edges, Social Networks **44**, 105 (2016).

[75] B. Kim, K. H. Lee, L. Xue, and X. Niu, A review of dynamic network models with latent variables, Stat. Surveys **12**, 105 (2018).

[76] P. Sarkar, S. M. Siddiqi, and G. J. Gordon, A latent space approach to dynamic embedding of co-occurrence data, in *Proceedings of the Eleventh International Conference on Artificial Intelligence and Statistics* (Proceedings of Machine Learning Research, San Diego, United States, 2007), pp. 420–427.

[77] P. Sarkar and A. W. Moore, Dynamic social network analysis using latent space models, in *Advances in Neural Information Processing Systems* (Curran Associates, Red Hook, United States, 2006), pp. 1145–1152.

[78] Y. Peres, A. Sinclair, P. Sousi, and A. Stauffer, Mobile geometric graphs: Detection, coverage and percolation, Probab. Theory Relat. Fields **156**, 273 (2013).

[79] A. Clementi and R. Silvestri, Parsimonious flooding in geometric random-walks, J. Comput. Syst. Sci. **81**, 219 (2015).

[80] H. Hartle, B. Klein, S. McCabe, A. Daniels, G. St-Onge, C. Murphy, and L. Hébert-Dufresne, Network comparison and the within-ensemble graph distance, Proc. R. Soc. A **476**, 20190744 (2020).

[81] J. R. Norris, *Markov Chains* (Cambridge University Press, Cambridge, United Kingdom, 1998).

[82] E. Behrends, *Introduction to Markov Chains*, Vol. 228 (Springer, Berlin, Germany, 2000).

[83] G. Bianconi, *Multilayer Networks: Structure and Function* (Oxford University Press, Oxford, United Kingdom, 2018).

[84] M. De Domenico, A. Solé-Ribalta, E. Cozzo, M. Kivelä, Y. Moreno, M. A. Porter, S. Gómez, and A. Arenas, Mathematical Formulation of Multilayer Networks, Phys. Rev. X **3**, 041022 (2013).

[85] P. T. Landsberg, Foundations of thermodynamics, Rev. Mod. Phys. **28**, 363 (1956).

[86] N. Perra, B. Goncalves, R. Pastor-Satorras, and A. Vespignani, Activity driven modeling of time varying networks, Sci. Rep. **2**, 469 (2012).

[87] F. Papadopoulos and M. A. R. Flores, Latent Geometry and Dynamics of Proximity Networks, Phys. Rev. E **100**, 052313 (2019).

[88] B. Bollobás, S. Janson, and O. Riordan, The phase transition in inhomogeneous random graphs, Random Struct. Alg. **31**, 3 (2007).

[89] R. I. Oliveira, Concentration of the adjacency matrix and of the Laplacian in random graphs with independent edges, arXiv:0911.0600.

[90] L. Lu and X. Peng, Spectra of edge-independent random graphs, arXiv:1204.6207.

[91] P. Erdos and A. Renyi, On random graphs I, Publ. Math. Debrecen **6**, 18 (1959).

[92] C. J. Anderson, S. Wasserman, and K. Faust, Building stochastic blockmodels, Social Networks **14**, 137 (1992).

[93] R. W. Hamming, Error detecting and error correcting codes, Bell Syst. Tech. J. **29**, 147 (1950).

[94] J. E. Steif, A survey of dynamical percolation, in *Fractal Geometry and Stochastics IV* (Springer, Berlin, Germany, 2009), pp. 145–174.

[95] Y. Peres and J. E. Steif, The number of infinite clusters in dynamical percolation, Probab. Theory Relat. Fields **111**, 141 (1998).

[96] D. Khoshnevisan, Dynamical percolation on general trees, Probab. Theory Relat. Fields **140**, 169 (2008).

[97] M. I. Roberts and B. Şengül, Exceptional times of the critical dynamical Erdős–Rényi graph, Ann. Appl. Probab. **28**, 2275 (2018).

[98] R. Rossignol, Scaling limit of dynamical percolation on critical Erdös-Rnyi random graphs, The Annals of Probability, **49**, 322 (2021).

[99] A. E. F. Clementi, C. Macci, A. Monti, F. Pasquale, and R. Silvestri, Flooding time of edge-Markovian evolving graphs, SIAM J. Discrete Math. **24**, 1694 (2010).

[100] J. Whitbeck, V. Conan, and M. D. de Amorim, Performance of opportunistic epidemic routing on edge-Markovian dynamic graphs, IEEE Trans. Commun. **59**, 1259 (2011).

[101] A. F. de Pebeyre, F. Tarissan, and J. Sopena, On the relevance of the edge-Markovian evolving graph model for real mobile networks, in *2013 IFIP Wireless Days (WD)* (IEEE, New York, United States, 2013), pp. 1–6.

[102] T. P. Peixoto, Entropy of stochastic blockmodel ensembles, Phys. Rev. E **85**, 056122 (2012).

[103] T. P. Peixoto, Nonparametric bayesian inference of the microcanonical stochastic block model, Phys. Rev. E **95**, 012317 (2017).

[104] S. G. Kobourov, Spring embedders and force directed graph drawing algorithms, arXiv:1201.3011.

[105] B. Söderberg, Random graphs with hidden color, Phys. Rev. E **68**, 015102(R) (2003).

[106] B. Söderberg, General formalism for inhomogeneous random graphs, Phys. Rev. E **66**, 066121 (2002).

[107] A. Allen-Perkins, Random spherical graphs, Phys. Rev. E **98**, 032310 (2018).

[108] D. J. Watts and S. H. Strogatz, Collective dynamics of 'small-world' networks, Nature **393**, 440 (1998).

[109] A. Buscarino, L. Fortuna, M. Frasca, and V. Latora, Disease spreading in populations of moving agents, Europhys. Lett. **82**, 38002 (2008).

[110] M. D. Penrose, Connectivity of soft random geometric graphs, Ann. Appl. Probab. **26**, 986 (2016).

[111] M. Wilsher, C. P. Dettmann, and A. Ganesh, Connectivity in one-dimensional soft random geometric graphs, Phys. Rev. E **102**, 062312 (2020).

[112] M. Kaiser and C. C. Hilgetag, Spatial growth of real-world networks, Phys. Rev. E **69**, 036103 (2004).

[113] C. P. Dettmann and O. Georgiou, Random geometric graphs with general connection functions, Phys. Rev. E **93**, 032313 (2016).

[114] I. Voitalov, P. van der Hoorn, M. Kitsak, F. Papadopoulos, and D. Krioukov, Weighted hypersoft configuration model, Phys. Rev. Research **2**, 043157 (2020).

[115] F. Chung and L. Lu, Connected components in random graphs with given expected degree sequences, Ann. Combinatorics **6**, 125 (2002).

[116] I. Norros and H. Reittu, On a conditionally Poissonian graph process, Adv. Appl. Probab. **38**, 59 (2006).

[117] K. Bringmann, R. Keusch, and J. Lengler, Average distance in a general class of scale-free networks with underlying geometry, arXiv:1602.05712.

[118] T. Friedrich and A. Krohmer, On the diameter of hyperbolic random graphs, SIAM J. Discrete Math. **32**, 1314 (2018).

[119] A. Faqeeh, S. Osat, and F. Radicchi, Characterizing the Analogy Between Hyperbolic Embedding and Community Structure of Complex Networks, Phys. Rev. Lett. **121**, 098301 (2018).

[120] G. García-Pérez, M. Boguñá, and M. Á. Serrano, Multiscale unfolding of real networks by geometric renormalization, Nat. Phys. **14**, 583 (2018).

[121] M. Kardar, *Statistical Physics of Particles* (Cambridge University Press, Cambridge, United Kingdom, 2007).

[122] X. Zhang, C. Moore, and M. E. J. Newman, Random graph models for dynamic networks, Eur. Phys. J. B **90**, 200 (2017).

[123] M. Mandjes, N. Starreveld, R. Bekker, and P. Spreij, Dynamic Erdős-Rényi graphs, in *Computing and Software Science* (Springer, Berlin, Germany, 2019), pp. 123–140.

[124] A. E. F. Clementi, F. Pasquale, A. Monti, and R. Silvestri, Information spreading in stationary markovian evolving graphs, in *2009 IEEE International Symposium on Parallel & Distributed Processing* (IEEE, New York, United States, 2009), pp. 1–12.

[125] R. Du, H. Wang, and Y. Fu, Continuous-time independent edge-Markovian random graph process, Chin. Ann. Math., Series B **37**, 73 (2016).

[126] I. Lamprou, R. Martin, and P. Spirakis, Cover time in edge-uniform stochastically-evolving graphs, Algorithms **11**, 149 (2018).

[127] L. Zino, A. Rizzo, and M. Porfiri, Continuous-Time Discrete-Distribution Theory for Activity-Driven Networks, Phys. Rev. Lett. **117**, 228302 (2016).

[128] I. Pozzana, K. Sun, and N. Perra, Epidemic spreading on activity-driven networks with attractiveness, Phys. Rev. E **96**, 042310 (2017).

[129] A. S. da Mata and R. Pastor-Satorras, Slow relaxation dynamics and aging in random walks on activity driven temporal networks, Eur. Phys. J. B **88**, 12 (2015).

[130] L. Alessandretti, K. Sun, A. Baronchelli, and N. Perra, Random walks on activity-driven networks with attractiveness, Phys. Rev. E **95**, 052318 (2017).

[131] A. Rizzo and M. Porfiri, Innovation diffusion on time-varying activity driven networks, Eur. Phys. J. B **89**, 20 (2016).

[132] M. Starnini and R. Pastor-Satorras, Temporal percolation in activity-driven networks, Phys. Rev. E **89**, 032807 (2014).

[133] A. Silvescu and V. Honavar, Temporal boolean network models of genetic networks and their inference from gene expression time series, Complex Syst. **13**, 61 (2001).

[134] S. Lebre, J. Becq, F. Devaux, M. P. H. Stumpf, and G. Lelandais, Statistical inference of the time-varying structure of gene-regulation networks, BMC Syst. Biol. **4**, 130 (2010).

[135] S. Hanneke, W. Fu, and E. P. Xing, Discrete temporal models of social networks, Electronic Journal of Statistics **4**, 585 (2010).

[136] A. Mellor, Event graphs: Advances and applications of second-order time-unfolded temporal network models, Adv. Complex Syst. **22**, 1950006 (2019).

[137] R. E. Miles, On the homogeneous planar poisson point process, Math. Biosci. **6**, 85 (1970).

[138] J. Møller and R. P. Waagepetersen, Modern statistics for spatial point processes, Scandin. J. Stat. **34**, 643 (2007).

[139] M. Reitzner, Poisson point processes: Large deviation inequalities for the convex distance, Electronic Communications in Probability **18**, 1 (2013).

[140] S. R. S. Varadhan, *Stochastic Processes* (American Mathematical Society, Providence, United States, 2007), Vol. 16.

[141] P. Mazzarisi, P. Barucca, F. Lillo, and D. Tantari, A dynamic network model with persistent links and node-specific latent variables, with an application to the interbank market, Eur. J. Operational Res. **281**, 50 (2020).

[142] R. Bian, Y. S. Koh, G. Dobbie, and A. Divoli, Network embedding and change modeling in dynamic heterogeneous networks, in *Proceedings of the 42nd International ACM SIGIR Conference on Research and Development in Information Retrieval* (Association for Computing Machinery, New York, United States, 2019), pp. 861–864.

[143] P. Goyal, S. R. Chhetri, N. Mehrabi, E. Ferrara, and A. Canedo, Dynamicgem: A library for dynamic graph embedding methods, arXiv:1811.10734.

[144] Y. Lu, X. Wang, C. Shi, P. S. Yu, and Y. Ye, Temporal network embedding with micro-and macro-dynamics, in *Proceedings of the 28th ACM International Conference on Information and Knowledge Management* (Association for Computing Machinery, New York, United States, 2019), pp. 469–478.

[145] Y. Xie, C. Li, B. Yu, C. Zhang, and Z. Tang, A survey on dynamic network embedding, arXiv:2006.08093.

[146] M. Haddad, C. Bothorel, P. Lenca, and D. Bedart, Temporalnode2vec: Temporal node embedding in temporal networks, in *International Conference on Complex Networks and Their Applications* (Springer, Berlin, Germany, 2019), pp. 891–902.

[147] D. Jin, S. Kim, R. A. Rossi, and D. Koutra, From static to dynamic node embeddings, arXiv:2009.10017.

[148] S. Spasov, A. Di Stefano, P. Lio, and J. Tang, Grade: Graph dynamic embedding, arXiv:2007.08060.

[149] C. Chen, Y. Tao, and H. Lin, Dynamic network embeddings for network evolution analysis, arXiv:1906.09860.

[150] P. Cheng, Y. Li, X. Zhang, L. Chen, D. Carlson, and L. Carin, Dynamic embedding on textual networks via a gaussian process, in *Proceedings of the AAAI Conference on Artificial Intelligence* (AIII Press, Palo Alto, United States, 2020), Vol. 34, pp. 7562–7569.

[151] L. Zhu, D. Guo, J. Yin, G. Ver Steeg, and A. Galstyan, Scalable temporal latent space inference for link prediction in dynamic social networks, IEEE Trans. Knowledge Data Eng. **28**, 2765 (2016).

[152] J. B. Lee, G. Nguyen, R. A. Rossi, N. K. Ahmed, E. Koh, and S. Kim, Dynamic node embeddings from edge streams, IEEE Trans. Emerging Top. Comput. Intelligence (2020).

[153] U. Singer, I. Guy, and K. Radinsky, Node embedding over temporal graphs, arXiv:1903.08889.

[154] S. Kumar, X. Zhang, and J. Leskovec, Learning dynamic embeddings from temporal interactions, arXiv:1812.02289.

[155] F. Papadopoulos, C. Psomas, and D. Krioukov, Network mapping by replaying hyperbolic growth, IEEE/ACM Trans. Networking **23**, 198 (2014).

[156] R. Pastor-Satorras, C. Castellano, P. Van Mieghem, and A. Vespignani, Epidemic processes in complex networks, Rev. Mod. Phys. **87**, 925 (2015).

[157] S. N. Dorogovtsev and J. F. F. Mendes, Evolution of networks, Adv. Phys. **51**, 1079 (2002).

[158] C. Moore, G. Ghoshal, and M. E. J. Newman, Exact solutions for models of evolving networks with addition and deletion of nodes, Phys. Rev. E **74**, 036121 (2006).

[159] H. Bauke, C. Moore, J.-B. Rouquier, and D. Sherrington, Topological phase transition in a network model with preferential attachment and node removal, Eur. Phys. J. B **83**, 519 (2011).

[160] L. Becchetti, A. Clementi, F. Pasquale, L. Trevisan, and I. Ziccardi, Expansion and flooding in dynamic random networks with node churn, arXiv:2007.14681.

[161] D. Krioukov and M. Ostilli, Duality between equilibrium and growing networks, Phys. Rev. E **88**, 022808 (2013).

[162] P. Van Mieghem, H. Wang, X. Ge, S. Tang, and F. A. Kuipers, Influence of assortativity and degree-preserving rewiring on the spectra of networks, Eur. Phys. J. B **76**, 643 (2010).

[163] J.-G. Young, G. Petri, F. Vaccarino, and A. Patania, Construction of and efficient sampling from the simplicial configuration model, Phys. Rev. E **96**, 032312 (2017).

[164] T. Bannink, R. van der Hofstad, and C. Stegehuis, Switch chain mixing times and triangle counts in simple random graphs with given degrees, J. Complex Networks **7**, 210 (2019).

[165] S. Bhamidi, G. Bresler, and A. Sly, Mixing time of exponential random graphs, in *2008 49th Annual IEEE Symposium on Foundations of Computer Science* (IEEE, New York, United States, 2008), pp. 803–812.

[166] R. DeMuse, T. Easlick, and M. Yin, Mixing time of vertex-weighted exponential random graphs, J. Comput. Appl. Math. **362**, 443 (2019).

[167] L. Avena, H. Güldaş, R. van der Hofstad, and F. den Hollander, Mixing times of random walks on dynamic configuration models, Ann. Appl. Probab. **28**, 1977 (2018).

[168] L. Avena, H. Güldaş, R. van der Hofstad, and F. den Hollander, Random walks on dynamic configuration models: a trichotomy, Stochastic Processes Appl. **129**, 3360 (2019).

[169] L. Avena, H. Güldaş, R. van der Hofstad, F. den Hollander, and O. Nagy, Linking the mixing times of random walks on static and dynamic random graphs, arXiv:2012.11012.

[170] T. Schlick, *Molecular Modeling and Simulation: An Interdisciplinary Guide: An Interdisciplinary Guide* (Springer Science & Business Media, Berlin, Germany, 2010), Vol. 21.

[171] M. A. R. Flores and F. Papadopoulos, Similarity Forces and Recurrent Components in Human Face-to-Face Interaction Networks, Phys. Rev. Lett. **121**, 258301 (2018).

[172] E. Jacob and P. Mörters, The contact process on scale-free networks evolving by vertex updating, R. Soc. Open Sci. **4**, 170081 (2017).

[173] H. Olle, P. Yuval, and E. S. Jeffrey, Dynamical percolation, in *Annales de l'Institut Henri Poincare (B) Probability and Statistics* (Elsevier, Amsterdam, Netherlands, 1997), Vol. 33, pp. 497–528.

[174] C. Garban, G. Pete, and O. Schramm, The scaling limits of near-critical and dynamical percolation, J. Eur. Math. Soc. **20**, 1195 (2018).

[175] K. E. Bassler, E. Frey, and R. K. P. Zia, Coevolution of nodes and links: Diversity-driven coexistence in cyclic competition of three species, Phys. Rev. E **99**, 022309 (2019).

[176] H. Sayama, I. Pestov, J. Schmidt, B. J. Bush, C. Wong, J. Yamanoi, and T. Gross, Modeling complex systems with adaptive networks, Comput. Math. Appl. **65**, 1645 (2013).

[177] K. Choromański, M. Matuszak, and J. Miȩkisz, Scale-free graph with preferential attachment and evolving internal vertex structure, J. Stat. Phys. **151**, 1175 (2013).

[178] G. Caldarelli, A. Capocci, and D. Garlaschelli, A self-organized model for network evolution, Eur. Phys. J. B **64**, 585 (2008).

[179] L. Papadopoulos, J. Z. Kim, J. Kurths, and D. S. Bassett, Development of structural correlations and synchronization from adaptive rewiring in networks of kuramoto oscillators, Chaos: Interdisciplinary J. Nonlinear Sci. **27**, 073115 (2017).

[180] RTAJ Leenders, Longitudinal behavior of network structure and actor attributes: Modeling interdependence of contagion and selection, Evol. Social Networks **1**, 165 (1997).

[181] Y.-H. Eom, S. Boccaletti, and G. Caldarelli, Concurrent enhancement of percolation and synchronization in adaptive networks, Sci. Rep. **6**, 27111 (2016).

[182] M. Mancastroppa, R. Burioni, V. Colizza, and A. Vezzani, Active and inactive quarantine in epidemic spreading on adaptive activity-driven networks, Phys. Rev. E **102**, 020301 (2020).

[183] G. Ichinose, Y. Satotani, H. Sayama, and T. Nagatani, Reduced mobility of infected agents suppresses but lengthens disease in biased random walk, arXiv:1807.01195.

[184] N. J. Gotelli, Research frontiers in null model analysis, Global Ecol. Biogeogr. **10**, 337 (2001).

[185] G. Siganos, M. Faloutsos, P. Faloutsos, and C. Faloutsos, Power laws and the as-level internet topology, IEEE/ACM Trans. Networking **11**, 514 (2003).

[186] L. Devroye, Nonuniform random variate generation, Handbooks Operations Res. Management Sci. **13**, 83 (2006).

[187] P. Billingsley, *Probability and Measure* (John Wiley & Sons, Hoboken, United States, 2008).

[188] F. Papadopoulos, M. Kitsak, M. Á. Serrano, M. Boguná, and D. Krioukov, Popularity versus similarity in growing networks, Nature **489**, 537 (2012).